JOURNAL OF GEOPHYSICAL RESEARCH, VOL. 103, NO. A7, PAGES 14,879–14,895, JULY 1, 1998

On the origin of the ion-electron temperature difference in the plasma sheet

D. Schriver, M. Ashour-Abdalla,[1] and R. L. Richard

Institute of Geophysics and Planetary Physics, University of California, Los Angeles

Abstract. The results of a study of proton and electron acceleration in the Earth's magnetotail are presented. By following the trajectories of thousands of charged particles launched from mantle and tail lobe source regions, distribution functions are calculated at different locations in a model magnetotail. The magnetic field is based on the *Tsyganenko* [1989] model combined with a constant cross-tail convection electric field. Despite the simplicity of the model and the lack of self-consistent fields, a qualitative picture of the proton/electron plasma sheet emerges including an ion to electron temperature ratio T_i/T_e ranging from about 4 to 6 in the magnetotail, in approximate agreement with plasma sheet observations. To explain this result, an analytic expression for T_i/T_e is derived based on the particle motion of ions and electrons in a current sheet configuration with a varying normal magnetic field component. The derived expression depends on the ion to electron mass ratio to the one-third power $(m_i/m_e)^{1/3}$ and a factor that takes the local field gradient into account. Using numerical values from the *Tsyganenko* [1989] field model in the derived equation gives $T_i/T_e \sim 5$. Another result is that the heated electron distribution functions formed in the plasma sheet are not Maxwellian but instead have power law high-energy tails much like the so-called "kappa" distributions reported by *Christon et al.* [1989]. At the edge of the plasma sheet, the calculations show the electron plasma sheet boundary layer extends further towards the lobe than the ion plasma sheet boundary layer, also in agreement with observations [*Takahashi and Hones*, 1988]. Nonisotropic distribution functions form at different locations in the plasma sheet, including electron beams streaming along field lines just inside the separatrix in the deep magnetotail. Electron distributions that are highly skewed in velocity space are found very near the magnetic null point. The nonisotropic distributions suggest that plasma instabilities and wave-particle interactions could occur in those regions. That such a simple model should reproduce many of the features of the observed plasma sheet indicates that adiabatic and nonadiabatic single-particle motion play important roles in the quiet time magnetotail and suggests that ion and electron plasma sheet formation is a natural consequence of single-particle motion in an X line type magnetotail geometry.

1. Introduction

The Earth's plasma sheet in the magnetotail is a region of relatively hot plasma with temperatures of the order of several keV and densities typically less than about 1 cm^3 [*Frank*, 1985]. Observations have established that in the plasma sheet the ion temperature is almost always greater than the electron temperature. *Slavin et al.* [1985] performed a statistical survey using ISEE 3 satellite data, and it was found that the ion to electron temperature ratio (T_i/T_e) varied between 4.8 and 7.8 in the deep magnetotail from 30 to 220 Earth radii (R_E) downtail. In the near-Earth magnetotail (< 20 R_E), a comprehensive statistical study of the plasma sheet using Active Magnetospheric Particle Tracer Explorers (AMPTE) satellite data showed that more than 80% of the particle data measurements fell within the range $5.5 < T_i/T_e < 11$, with a best fit in the inner central plasma sheet of $T_i = 7.8\ T_e$ [*Baumjohann et al.*, 1989]. Data from the Geotail satellite in the deep magnetotail shows that on average $T \gtrsim 5T_e$ [*Paterson and Frank*, 1994].

Observed distribution functions of ions and electrons in the central plasma sheet (CPS) are in general isotropic with ion temperatures ranging from 1 to 10 keV [*Frank et al.*, 1976; *Eastman et al.*, 1984; *Takahashi and Hones*, 1988]. A close analysis of particle energy profiles using ISEE satellite data showed that the best fits to the distributions were those with a power law high-energy tail, such as a "kappa" distribution, rather than a strict Maxwellian [*Christon et al.*, 1988, 1989]. At the edge of the plasma sheet near the lobe is a region known as the plasma sheet boundary layer (PSBL), where field-aligned ion beams streaming earthward and tailward are commonly observed [*Frank et al.*, 1976; *DeCoster and Frank*, 1979; *Parks et al.*, 1984; *Eastman et al.*, 1984; *Takahashi and Hones*, 1988]. At the outermost edge of the PSBL, hot electrons and electron beams extend beyond the ion PSBL towards the lobe [*Parks et al.*, 1984; *Takahashi and Hones*, 1988; *Schriver et al.*, 1990; *Onsager et al.*, 1990]. The electron PSBL is on closed field lines just inside the separatrix between open lobe and closed plasma sheet field lines [*Takahashi and Hones*, 1988].

[1]Also at Department of Physics and Astronomy, University of California, Los Angeles.

Paper number 98JA00017.
0148-0227/98/98JA-00017$09.00

Although these plasma measurements form a well-established observational picture of the Earth's plasma sheet, surprisingly little theoretical work has been done to explain the formation of the electron plasma sheet that includes the differences found between ions and electrons. For example, the origin of the temperature ratio of ions and electrons in the plasma sheet is not known, and investigators [e.g., *Frank*, 1985] believe it is associated with the primary plasma acceleration mechanisms operating in the magnetotail. The origin of high-energy tails in the electron and proton distribution functions is also not well understood but again is probably associated with basic plasma energization processes [*Christon et al.*, 1988, 1989].

One of the problems in understanding the formation of the plasma sheet is that it is difficult to include both ion and electron dynamics in a single global simulation. Magnetohydrodynamic (MHD) simulations have been very successful in modeling global magnetospheric structure in response to the solar wind, including the formation of a plasma sheet with enhanced pressure in the magnetotail [*Raeder et al.*, 1995; *Fedder et al.*, 1995; *Tanaka*, 1995; *Spicer et al.*, 1996; *Walker and Ogino*, 1996]. But because the single fluid MHD description deals only with the moments of the distribution function, the difference between electron and ion temperatures and non-Maxwellian features such as beams and high-energy tails in the distribution function cannot be explained in that framework. Numerical calculations in which ion trajectories are followed in large-scale global magnetic field configurations either from empirical models or MHD simulations have been very successful in describing ion distributions in the plasma sheet and have illuminated the important role of nonadiabatic motion in the magnetotail [*Ashour-Abdalla et al.*, 1990, 1991a, 1993, 1996a, 1997; *Delcourt et al.*, 1990, 1995, 1996a, b; *Delcourt and Moore*, 1992; *Delcourt and Martin*, 1994; *Birn and Hesse*, 1994; *Joyce et al.*, 1995; *El-Alaoui et al.*, 1998]. In these studies, however, only ion motion was considered.

One study in which both ions and electrons were examined was the model of *Onsager et al.* [1990, 1991]. Starting with protons and electrons in the deep magnetotail that had initial Maxwellian distributions with temperatures typical of those observed in the plasma sheet (~keV), distributions were calculated in a parabolic field line model of the near-Earth CPS and PSBL. It was found that, due to time-of-flight effects, ion and electron beam-like cutoff distribution functions were formed in the PSBL, while in the CPS the distributions became more isotropic near the Earth, in agreement with observations. Also, it was found that the electron PSBL extended further outwards (towards the lobe) than the ion PSBL. The results of *Onsager et al.* [1990, 1991] made it clear that some basic features of the plasma sheet could be explained by adiabatic motion and time-of flight effects; however, they did not consider how the relatively cool source plasma from outside the closed field line region of the magnetotail is initially energized to form the deep tail plasma sheet, and their model did not include nonadiabatic effects. The cause of the observed T_i/T_e in the plasma sheet and high-energy tails of the distributions were not explained.

Although the details of nonadiabatic particle motion in the magnetotail current sheet has focused on ions [*Speiser*, 1965a, b; *Dungey*, 1968; *Cowley*, 1978, 1984; *Lyons and Speiser*, 1982; *Chen and Palmadesso*, 1986; *Büchner and Zelenyi*, 1986, 1989; *Martin*, 1986; *Ashour-Abdalla et al.*, 1990, 1993; *Chen*, 1992], electrons can also exhibit nonadiabatic motion under certain magnetic field conditions [*Speiser*, 1965a; *Cowley*, 1984; *Lyons*, 1984; *Zelenyi et al.*, 1990]. Near an X line type null region of the magnetic field, electrons can be strongly accelerated by a cross-tail electric field forming highly skewed distributions in velocity space [*Dungey*, 1988; *Lyons and Pridmore-Brown*, 1990, 1992; *Schriver and Ashour-Abdalla*, 1994, 1995; *Smets et al.*, 1996], an effect also seen for ions near an X line [*Martin and Speiser*, 1988]. Further from the X line in the magnetotail midplane a heated electron central plasma sheet begins to form and just inside the magnetic separatrix on closed field lines a field-aligned electron beam is created [*Schriver and Ashour-Abdalla*, 1994, 1995]. These studies, however, were done for regions relatively close to the magnetic null point, and the consequences for the plasma sheet as a whole and comparisons with ions were minimal.

In this paper we discuss the results from a simple model of plasma sheet formation which includes both ions and electrons. Our approach is to follow the trajectories of thousands of initially relatively cool protons and electrons ($\leq$ 300 eV) launched from source regions such as the mantle and lobe in a magnetic field model representative of the Earth's magnetosphere. The advantage of this approach is that particle kinetics on a global scale can be examined, but at the cost of losing the self-consistent feedback of the particles on the fields. Thus the particles move about on individual trajectories having no interactions with other particles and no feedback on the global fields. While it might be argued that following noninteracting ion trajectories in a global field model is reasonable because ions are relatively heavy and less responsive to plasma wave fields, this assumption might be questionable for electrons. This is because electrons could be strongly affected by plasma waves and ambipolar fields due to ion and electron spatial charge separation which would affect plasma transport. Nevertheless, we attempted the calculation with electrons to see if we could reproduce some of the observed results. We will then attempt to assess whether this was a useful exercise a posteriori.

This paper is organized as follows. In the next two sections the details of the model are discussed and the magnetic field configuration is presented. In section 4 the particle trajectory results are presented. In section 5 an analytic expression for the ion to electron temperature ratio is derived for a magnetotail-like field configuration. The paper is concluded in section 6 with a summary and implications for the magnetotail.

2. Particle Tracing Model

The particle tracing scheme used in our calculation is very straightforward. Thousands of individual charged particle trajectories are followed in a global field model subject to the Lorentz force equation:

$$m\frac{d\mathbf{v}}{dt} = q\mathbf{E} + q\mathbf{v}\times\mathbf{B} \tag{1}$$

Here the electric and magnetic fields $\mathbf{E}$ and $\mathbf{B}$ are specified throughout the spatial domain open to the particles and are constant in time. The particle charge and mass enter through q and m, respectively. The above equation is solved for the particle velocity $\mathbf{v}$ at each time step using the fourth-order Runge-Kutte numerical scheme [e.g., *Press et al.*, 1989]. It should be noted that (1) is used for both ions and electrons, that is, approximations such as the adiabatic guiding center equations [*Northrup*, 1963] are not used for either species since it is not certain a priori where the motion might be nonadiabatic.

In order to follow either ion or electron trajectories using (1), a small enough time step must be used such that convergence is achieved. This is done by using a time step Δt such that $\Omega\Delta t << 1$, where Ω is the relevant (ion or electron) cyclotron frequency. Since the gyrofrequency is given by qB/m, which is proportional to the magnetic field B, care must be taken when choosing the time step since the magnetic field is spatially variable in the system. To avoid wasting valuable computation time by using too small a time step in regions where it is not needed, a variable time step can be used such that $\Omega\Delta t \approx 0.05$ at all locations. But the trade-off for using a variable time step is that testing has to be done constantly for each particle to determine whether the time step needs to be changed or not. In the end, it was found to be more economical to use a fixed time step which at some locations might be smaller than necessary but overall would lead to energy conservation throughout the particle's trajectory. For electrons a value of of $\Omega\Delta t = 0.0015$ (at 80 R_E in the magnetotail midplane) was found through trial and error to be a reasonable time step in which energy was conserved. When electrons get near the Earth (within about 10 R_E), computation time increases dramatically since the magnetic field strength increases; however, a near-Earth boundary of 5 R_E was used, and it turned out that only a small number of electrons actually got within the near-Earth region between 5 and 10 R_E.

After many thousands of particles have been followed, distribution functions can be constructed at any location within the spatial domain as long as enough particles are used such that statistically meaningful distribution functions can be formed [*Ashour-Abdalla et al.*, 1996b]. Storing all of the particle trajectory data for every particle is both impractical and unnecessary. Instead, virtual detectors are placed at strategic locations within the spatial domain and distribution functions and their moments can then be calculated at the virtual detectors. A detailed description of how the distribution functions are calculated using virtual detectors is given by *Ashour-Abdalla et al.* [1993]; we used the exact same method as discussed in that paper.

A Cartesian coordinate system is used here with x along the Sun-Earth line positive in the tailward (antisunward) direction, y along the dawn-dusk line with positive y in the dawnward direction, and z along the north-south direction with positive z pointing northward. The global magnetic field is taken from the *Tsyganenko* [1989] empirical magnetic field model and is stored in a table which contains the field components at different grid locations. A two-dimensional reduction of the *Tsyganenko* [1989] field model is used in the x–z plane at $y = 0$, with no variation considered in the y direction (although particles are allowed to move in all three dimensions). The field is interpolated from the nearest grid points to find the value of the field at the particle location. A grid point resolution of 0.02 R_E is used in the x–z direction (in an x, y, z Cartesian coordinate system). The use of a table was found to be much faster computationally than calculating the magnetic field value at each particle's location using the *Tsyganenko* [1989] field model. The table is generated initially and once created is accessed by the main program as needed. For simplicity a constant cross-tail convection electric field of $E_y = -0.25$ mV/m (pointing dawn to dusk) is used, which for the two-dimensionally reduced *Tsyganenko* [1989] magnetic field model at $y = 0$ results in no parallel electric fields being present in the system. Other trajectory tracing calculations have considered the case of three-dimensional magnetic fields and nonuniform electric field for ions [*Joyce et al.*, 1995; *Peroomian and Ashour-Abdalla*, 1996; *Ashour-Abdalla et al.*, 1997; *El-Alaoui et al.*, 1998].

Using the two-dimensional reduction of the *Tsyganenko* [1989] model in the x–z plane raises some concerns about the requirement that $\nabla \cdot B = 0$. It was found that tailward of about 10 R_E and/or in the magnetic equator, $\nabla \cdot B \approx 0$ is satisfied for all z values considered in this study (see *Ashour-Abdalla et al.* [1994] for complete quantitative details concerning this issue). Earthward of 10 R_E, the magnetic field becomes more dipolar, and within 5 R_E it is clear that $\nabla \cdot B \neq 0$. The earthward cutoff of our system is taken to be at 5 R_E in x, and for the small fraction of particles that traveled earthward of 10 R_E, we monitored their energies for conservation. Most of these particle were at relatively large z values (> 3 to 5 R_E), where this problem is not severe. Nevertheless, any "bad" particles which did not conserve energy were removed from the system; however; it turned out that very few particles had to be removed. Our main results in this paper are concerned with the magnetotail at distances about 30 R_E and tailward.

The spatial domain of the system for the particles covers the magnetotail with ranges given by $5 \leq x/R_E \leq 120$, $-25 \leq y/R_E \leq 25$, and $15 \leq z/R_E \leq -15$. Protons and electrons are launched from the nominal mantle region at $x = 15$ R_E and $|z| = 7$ to 15 R_E (from both hemispheres) with an initially Maxwellian velocity distribution with a temperature of 300 eV and field-aligned tailward drift speeds of 200 km/s. The mantle was discussed as a source of plasma for the plasma sheet by *Pilipp and Morfill* [1978]. Particles for the mantle source are initially assigned randomized velocities to fit a Maxwellian distribution function in three velocity dimensions such that the initial pitch angle distribution is isotropic and the velocities fall within the usual Gaussian type curve with a thermal spread that corresponds to the initial temperature of 300 eV. There is some favoring of smaller pitch angles due to the initial field-aligned drift that is added to be consistent with a mantle distribution. For electrons the thermal speed is much larger than the field-aligned drifts, so this effect is negligible, while for ions, since the drift speed is comparable to the thermal speed, this effect is more pronounced.

Protons and electrons were also launched from the lobe region at different locations from $x = 80$ to 120 R_E and $z = \pm 2$ R_E with an initial temperature of 100 eV. These particles probably originate either in the ionosphere and flow out along open field lines as part of the polar wind [*Banks and Holzer*, 1968; *Chappell et al.*, 1987] or are of solar wind origin entering the magnetosphere from the deeper tail along open field lines [*Baker et al.*, 1986]. The initial temperature of 100 eV we use is based on lobe temperatures measured in the deep magnetotail at $x \sim 100$ R_E by *Slavin et al.* [1985]. Like the mantle, the lobe particles initially are randomized in velocity to fit a Maxwellian distribution which is isotropic in pitch angle, except here a 100 eV thermal width is used and there is no initial field-aligned drift. The reason for using another source region different from the mantle source was because it was found that although a large number of ions would flow into the magnetotail plasma sheet from our chosen mantle location, very few electrons would make it from the mantle. From the lobe source, however, both ions and electrons populate the plasma sheet.

Since our model is two-dimensional in x–z, with no variation in y, we did not consider a low-latitude boundary layer (LLBL) source in this study, which can be a contributor to the plasma sheet [*Eastman et al.*, 1985]. Future studies with a three-dimensional field model should include an LLBL source in addition to the other sources used in this study.

The magnetic field lines in the x–z (Sun-Earth, north-south plane) are shown in Figure 1 along with dark bars representing

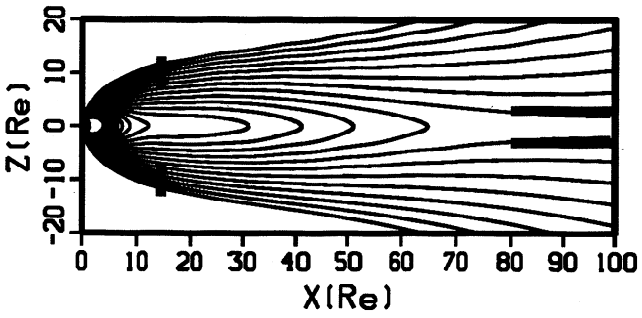

Figure 1. Magnetic field lines from the *Tsyganenko* [1989] model are plotted in the x–z plane. The Earth is to the left and positive x is in the tailward direction. A magnetic null point (X line) occurs at $x = 100\ R_E$. The dark solid bars represent the launch points of the source plasma in the mantle and lobe region.

the source regions from where the particles are launched. At the different launch points the particles initially have adiabatic trajectories. The motion is primarily field aligned combined with transverse drift towards the magnetotail midplane due to cross-tail $\mathbf{E} \times \mathbf{B}$ convection. When a particle reaches any of the boundaries in the x, y, z direction, it is considered lost from the system.

3. Magnetic Field Model

As mentioned in the previous section, the *Tsyganenko* [1989] magnetic field model was used for these calculations. Before empirical models of the Earth's magnetosphere were first developed [e.g., *Mead and Fairfield*, 1975], most particle trajectory tracing calculations were performed using relatively simple analytic current sheet representations [*Speiser*, 1965b; *Lyons and Speiser*, 1982; *Büchner and Zelenyi*, 1986, 1989; *Chen and Palmadesso*, 1986; *Martin*, 1986]. These calculations demonstrated the importance of nonadiabatic motion. The more sophisticated *Zwingman* [1983] analytic field model of the magnetotail was used by *Ashour-Abdalla et al.* [1990, 1991b] to understand magnetotail particle motion on a more global scale, and the *Mead and Fairfield* [1975] model was used by *Delcourt et al.* [1990] to study single particle motion during substorm expansion. The *Tsyganenko* [1989] field model was used for particle trajectory tracing for the first time by *Ashour-Abdalla et al.* [1991a]. Since then other field models have been used such as the *Tsyganenko and Usmanov* [1982] model, the *Tsyganenko* [1987] model and its variants [*Delcourt and Moore*, 1992; *Delcourt and Martin*, 1994; *Delcourt et al.*, 1995, 1996a, b], and electric and magnetic fields from global MHD simulations [*Birn and Hesse*, 1994; *Richard et al.*, 1994; *Joyce et al.*, 1995; *Walker et al.*, 1996; *Ashour-Abdalla et al.*, 1997; *El-Alaoui et al.*, 1998]. Analytic field models are also still used to understand basic physics of particle motion in the magnetotail current sheet [*Usadi et al.*, 1996], including time-varying fields [*Chapman and Watkins*, 1993; *Chapman*, 1993, 1994].

The choice of using the *Tsyganenko* [1989] field model here is motivated by three requirements: (1) the desire to use a reasonable qualitative representation of the Earth's quiet time magnetotail, (2) ease of use in the numerical calculations, and (3) the ability to compare with previous trajectory calculations. The *Tsyganenko* [1989] model (which for shorthand will be referred to hereinafter as T89) satisfies these requirements.

A data based empirical field model reflects an average state of the magnetosphere because the data used are often taken over a period of months or years and possibly by different satellites. The data for the T89 model are binned into different magnetic activity levels depending on the Kp index. Although the T89 model may overestimate or underestimate the magnetic field strength at certain locations of the magnetotail compared to particular satellite data sets [*Peredo et al.*, 1993], it has characteristic qualitative features which fit with an expected quiet time average magnetotail that has a normal magnetic field (B_Z) in the magnetotail midplane that decreases with distance away from the Earth. Figure 2 shows the value of the T89 normal field component B_Z at $z = 0$ versus x (downtail distance). The value of B_Z can be seen to decrease to zero at about $100\ R_E$. For comparison the average magnetic field value versus downtail distance measured by the ISEE 3 satellite from *Slavin et al.* [1985] is also shown in Figure 2. Although this comparison shows that the T89 field at a given x location underestimates the normal field value with respect to the ISEE 3 data, the trend is similar in that the magnetic field decreases down the magnetotail to very low values. If the T89 magnetic minimum were relocated to $120\ R_E$ keeping the same slope, the fields would match well. Thus the T89 model represents a reasonable model of a quiet time magnetotail which has a decreasing normal magnetic field component. While a magnetic null point may not occur at exactly $100\ R_E$, an X line somewhere in the magnetotail could be common. Future studies with newer or modified field models [e.g., *Peredo et al.*, 1993, *Tsyganenko and Stern*, 1996] should clarify this point. Note that in Figure 2 the observed magnetic field can drop to less than 0.1 nT, which is the approximate threshold below which electrons have nonadiabatic trajectories [*Zelenyi et al.*, 1990]. We therefore can expect nonadiabatic behavior from electrons as well as ions.

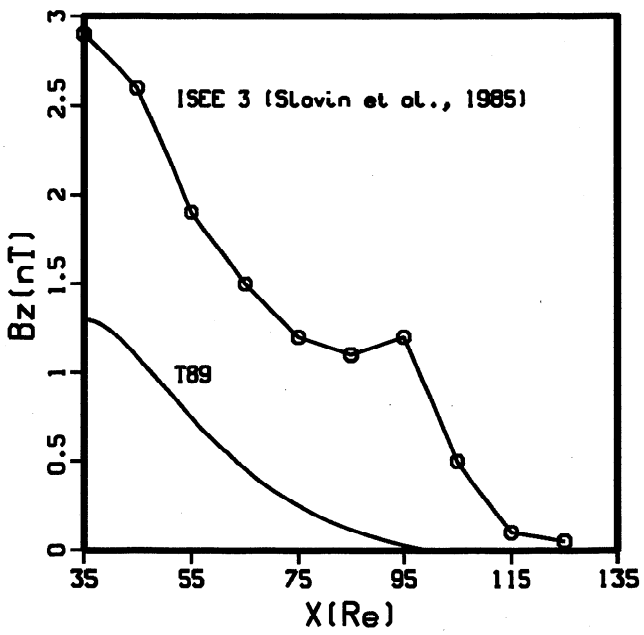

Figure 2. Plot of the normal magnetic field (B_Z) in the magnetotail midplane versus x. The smooth line labeled T89 is taken from the *Tsyganenko* [1989] magnetic field model, while the line with circles is constructed using data from the ISEE 3 satellite from *Slavin et al.* [1985]; the circles represent average data points.

The second criteria for choosing the T89 model was ease of use. As discussed in the previous section, the field values are stored in a table which is used by the particle trajectory tracing program. The options used in the T89 field generating program for the results presented here are zero magnetic dipole tilt and an iopt value of 2, which corresponds to a *Kp* index of –1, 1, 1+ (low magnetic activity).

The third criteria is comparison with previous results. The T89 has been used in many studies of ion trajectories in the Earth's magnetosphere [*Ashour-Abdalla et al.*, 1991a, 1992, 1993, 1994, 1996a, b; *Bosqued et al.*, 1993; *Delcourt and Martin*, 1994; *Peroomian and Ashour-Abdalla*, 1996; *Delcourt et al.*, 1996a, b]. These studies have been very successful in understanding ion acceleration in the magnetotail and transport in general. The results presented here for the ions essentially reproduce what was found in these previous studies. The novel aspect of this work is to compare the results with electron motion using the same magnetotail model.

4. Particle Trajectory Results

Most of the results shown in this section will be from virtual detectors placed at different locations in the model magnetotail. Figure 3 shows the virtual detector locations for the results presented in this section together with the field lines of the T89 model in the magnetotail region. The numerical data from the virtual detectors typify the major results of this study. As seen in Figure 3, most of the virtual detectors presented in this section are y–z planes at different x locations down the magnetotail. One additional virtual detector is placed in the x–y plane at $z = 0$, which is at the middle of the CPS.

We begin by discussing results closer to the Earth at $x = 30\ R_E$ and then move tailward. Figure 4 shows phase space density in z–v_x space for ions on the left panel and for electrons on the right panel. Note that z is in units of R_E and v_x is in units of km/s and darker shading corresponds to regions of higher density. To understand this type of plot, keep in mind that z is the north-south direction and v_x is velocity in the Sun-Earth direction, with negative v_x corresponding to earthward flow and positive v_x representing flow in the tailward direction. From Figure 4 it can immediately be seen that the overall shape of the phase distributions are different for ions and electrons. The left panel of Figure 4 essentially reproduces Figure 1 of *Ashour-Abdalla et al.* [1991a] and it can be seen that around $z = 0$ in the magnetotail midplane a heated CPS is formed [*Ashour-Abdalla et al.*, 1993], while at $z \approx \pm R_E$ strong earthward and tailward ion beams are formed. Because the field lines are approximately

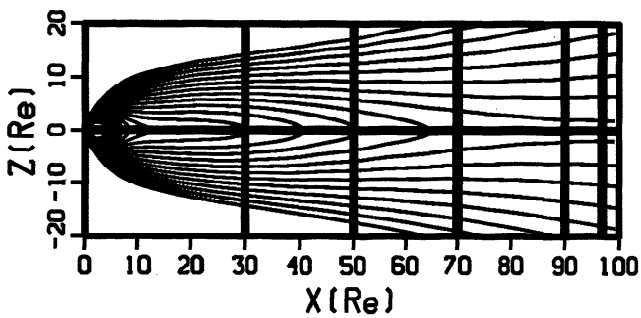

Figure 3. Virtual detectors superimposed on the *Tsyganenko* [1989] field model are shown. A virtual detector at $z = 0$ was also used for this study.

along the x direction at higher $|z|$ values (see Figure 3), the ion phase space plot shows that the plasma flow at $z = \pm 5\ R_E$ is field aligned, typical of the PSBL. The results in the right panel of Figure 4 show that the electrons also display a heated CPS with temperatures highest at $z = 0$ and at $z \approx 6\ R_E$ earthward and tailward field-aligned particles are found, again typical of the PSBL. The differences in the overall look of the ion and electron phase space distributions occurs because at 30 R_E ions are still within or just earthward of the region where the dominant particle motion is nonadiabatic. Electrons, on the other hand, are strongly adiabatic in this region of the magnetotail even though the electron distribution contains many electrons that were originally accelerated nonadiabatically in the deep magnetosphere as we shall see later. At 30 R_E the resulting electron phase space is due primarily to time of flight effects as discussed by *Onsager et al.* [1990, 1991].

It can also be seen in Figure 4 that the electron PSBL extends to higher $|z|$ values than the ion PSBL. While the ion PSBL cuts off at about 5.5 R_E in z, the electron PSBL extends to $z = 7\ R_E$. The electrons are just inside the magnetic separatrix between open and closed field lines, while ions are further from the separatrix. Thus if a satellite were coming from the lobe region on open field lines moving towards the magnetotail midplane, it would first encounter high-energy electrons indicative of the electron PSBL and then field-aligned streaming PSBL ion beams. This is in agreement with observations [*Takahashi and Hones*, 1988] and time of flight motion from an energized plasma source in the magnetotail tailward of 30 R_E [*Onsager et al.*, 1990].

The energy distribution of electrons in the CPS at $x = 30\ R_E$ and $z = 0$ is shown in Figure 5. Plotted is particle flux versus energy in keV, both axes on a log scale. This is in the same format as ISEE satellite data presented by *Christon et al.* [1988, 1989] for comparison. The results from the particle trajectory tracing are shown by the solid line along with a Maxwellian fit to the distribution by the dashed line and a power law type distribution, which *Christon et al.* [1988] used called the "kappa" distribution, shown by the chain dash line. The temperature used for the Maxwellian distribution was 660 eV, while the kappa distribution is shown for a kappa value of 5.0 and a peak energy of 660 eV. It can be seen that the kappa distribution is the better fit to the numerical results. This is in approximate agreement with the electron CPS distributions observed by *Christon et al.* [1989] who used ISEE satellite data and found that during undisturbed times kappa values ranged from 4 to 8 with the most probable values being about 5 to 6. The buildup of the kappa distributions appears to occur at distances tailward of 70 R_E, since even at that location (70 R_E) distributions exhibit kappa-like power law high-energy tails. Tailward of this region is where electron motion is nonadiabatic. Since the bulk of the energetic electrons earthward of 70 R_E are particles that were originally accelerated by nonadiabatic processes tailward of 70 R_E which then convect earthward, it would appear that a combination of the two types of motion can create these types of distributions. It is difficult to separate the two motions (adiabatic and nonadiabatic), however, and thus it is unclear exactly how the distributions form as a result of this combined motion.

Phase space contours for ions and electrons at $x = 50\ R_E$ are shown in Figure 6 in a format similar to Figure 4. The main features are similar to those at $x = 30\ R_E$ with a different overall shape of the phase space distribution for ions and electrons.

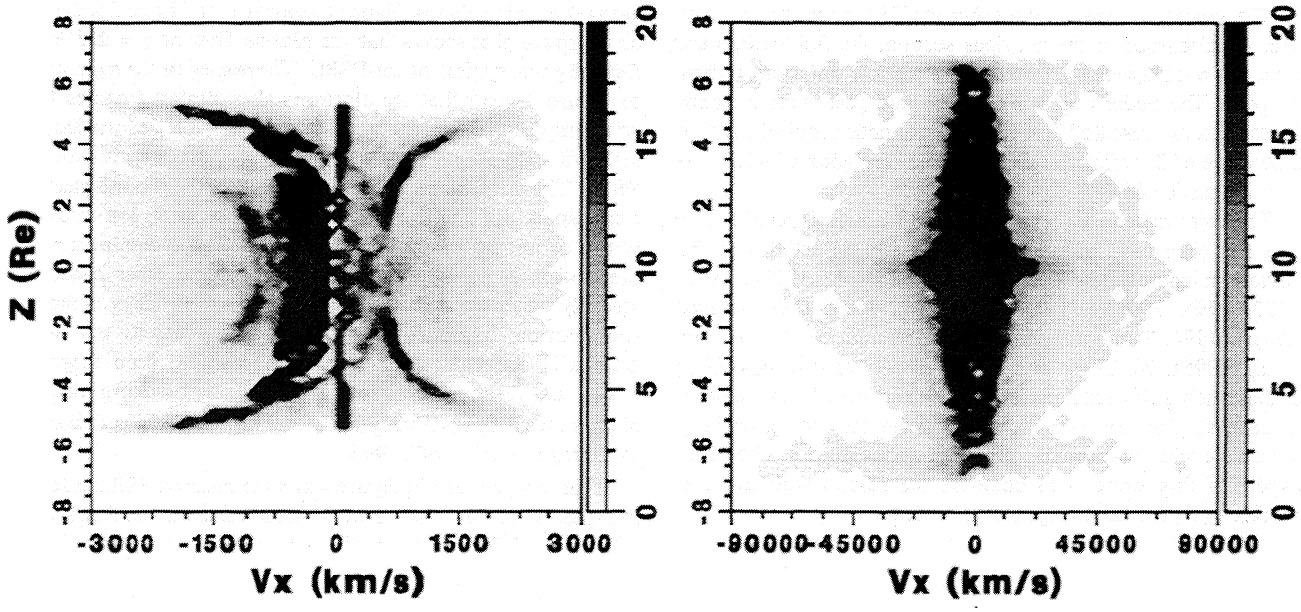

Figure 4. Phase space contours at $x = 30\ R_E$ in the magnetotail are shown for (left) ions (protons) and (right) electrons plotted in z–v_x, where z is in units of R_E and v_x is in units of km/s. Thus $z = 0$ corresponds to the magnetotail midplane and v_x represents velocity either earthward ($-v_x$) or tailward ($+v_x$). The shading is such that darker regions correspond to higher phase density.

Both species have a heated CPS at $z = 0$ and a distinctive PSBL at $z \approx \pm 4\ R_E$. The electrons, as before, extend to higher $|z|$ values closer to the separatrix than ions. The PSBL overall is at smaller $|z|$ values compared to $x = 30\ R_E$ since the closed field line region itself is narrowing down to the magnetic null region at $x = 100\ R_E$, as seen in Figure 3. The ion phase space also shows a distinctive solid line of cool tailward flowing particles with $v_x \approx 200$ km/s which are simply the mantle source particles crossing into the closed field line region for the first time. Most of these particle cross $z = 0$ tailward of $x = 50\ R_E$. Electron energy distributions (not shown) are again best fit to a power law type distribution with kappa value of about 5 to 6, similar to that found at $x = 30\ R_E$.

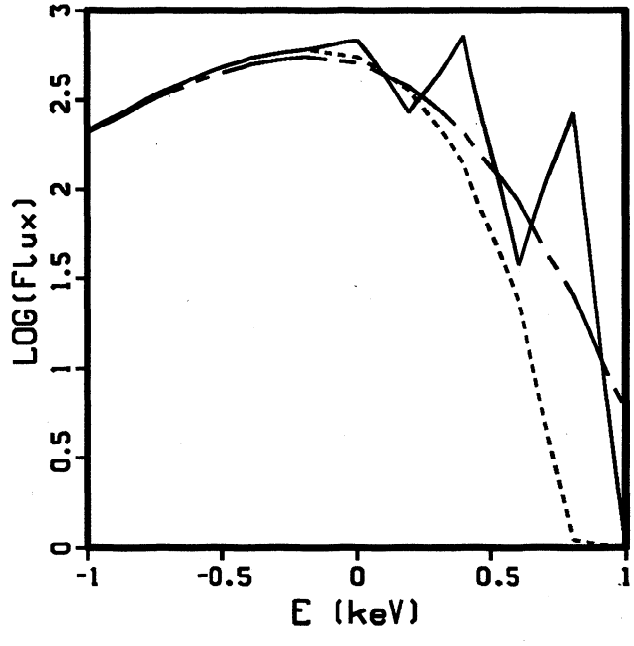

Figure 5. Energy distribution of electrons at $x = 30\ R_E$ in the central plasma sheet at $z = 0$. Shown is flux versus energy (in keV), both plotted on a log scale. Three lines are shown on each graph: the solid line is from the numerical calculations, the dashed line is a best fit to the distribution using a Maxwellian, and the chain dash line is a best fit to a kappa distribution. The form used for the kappa distribution was taken from *Christon et al.* [1988]. The parameters used for the kappa distribution are a kappa value of 5.0 and a peak energy of 660 eV.

Further down the magnetotail at $x = 70\ R_E$, the phase space contour in Figure 7 shows the ion and electron phase space distributions changing quite a bit. The ions show the formation of a "proto" plasma sheet as discussed by *Ashour-Abdalla et al.* [1993] which has the cross-patch interlace look due to the nonadiabatic interactions that occur in this region. Electrons, on the other hand, still maintain the look of a plasma sheet type structure, but the overall shape is different from that seen for electrons at $x = 30$ and $50\ R_E$. A transition from predominantly adiabatic electron motion earthward of $70\ R_E$ to increasingly non-adiabatic electron motion tailward of $70\ R_E$ is occurring at this point.

At $x = 90\ R_E$, near the magnetic null point at $100\ R_E$, the electrons are definitely in a region where nonadiabatic motion dominates. This can be seen in Figure 8, which shows the electron phase space contours on the left (z versus v_x in a format similar to Figures 4 and 6) and a plot of velocity space taken at $x = 90\ R_E$ and $z \approx 0.8\ R_E$ on the right. The phase space contours for the electrons in the left panel look very similar to the structure of the ion phase space contours at $x = 30$ and $50\ R_E$ with a heated CPS around $z = 0$ and strong field-aligned flow in the PSBL at higher $|z|$ values. As was the case for the ions at $x = 30\ R_E$, the overall shape of the electron phase space contour is due to nonadiabatic motion near and tailward of $90\ R_E$. The PSBL velocity space diagram on the right panel of Figure 8 shows clearly the field-aligned electron beam streaming earthward. The cool core distribution near $v_x = 0$ seen in both

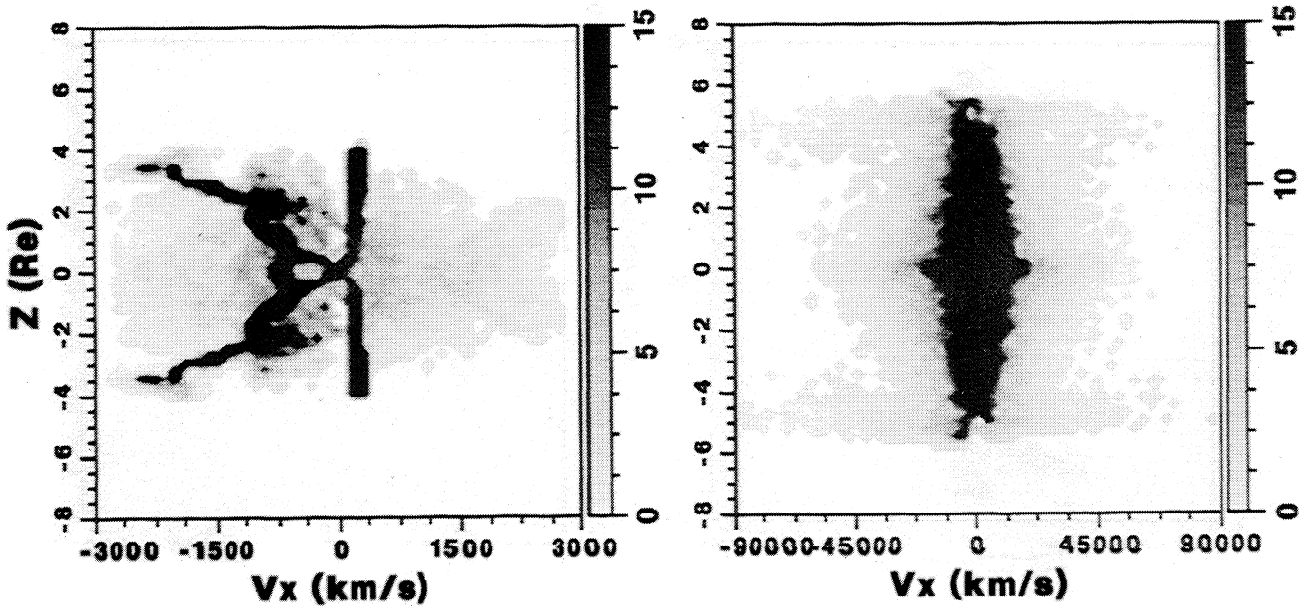

Figure 6. Phase space contours at $x = 50\ R_E$ in the magnetotail for (left) ions and (right) electrons. They are plotted in the z–v_x plane in the same format as Figure 4. The shading is such that darker regions correspond to higher phase density.

panels of Figure 8 are electrons just entering the closed field line region which have not been strongly accelerated, which is a feature similar to that seen for ions in Figure 6. An earthward streaming electron beam in the PSBL near an X line has been seen in previous studies [*Schriver and Ashour-Abdalla*, 1995; *Smets et al.*, 1996], and in a simple linear analysis the distribution was shown to be unstable to a Buneman type streaming mode with frequencies near the electron plasma frequency [*Schriver and Ashour-Abdalla*, 1995]. The electron beam could be unstable to electrostatic solitary waves (ESW) and become a source of observed broadband electrostatic noise in the PSBL detected by the Geotail satellite [*Matsumoto et al.*, 1994; *Omura et al.*, 1994, 1996], although detailed calculations of this are beyond the scope of this paper.

Very close to the magnetic null point the electrons are highly nonadiabatic as can be seen in Figure 9, which shows (in a similar format to Figure 8) phase space contours on the left and velocity space at $z = 0$ on the right. The phase space contours show that electrons are jetting earthward away from the X line and the velocity space contour shows the highly skewed distribution in velocity space first predicted analytically by *Dungey* [1988] and then found numerically in a number of studies [*Lyons and Pridmore-Brown*, 1990, 1992; *Schriver and Ashour-Abdalla*, 1994, 1995; *Smets et al.*, 1996]. Detailed discussion of

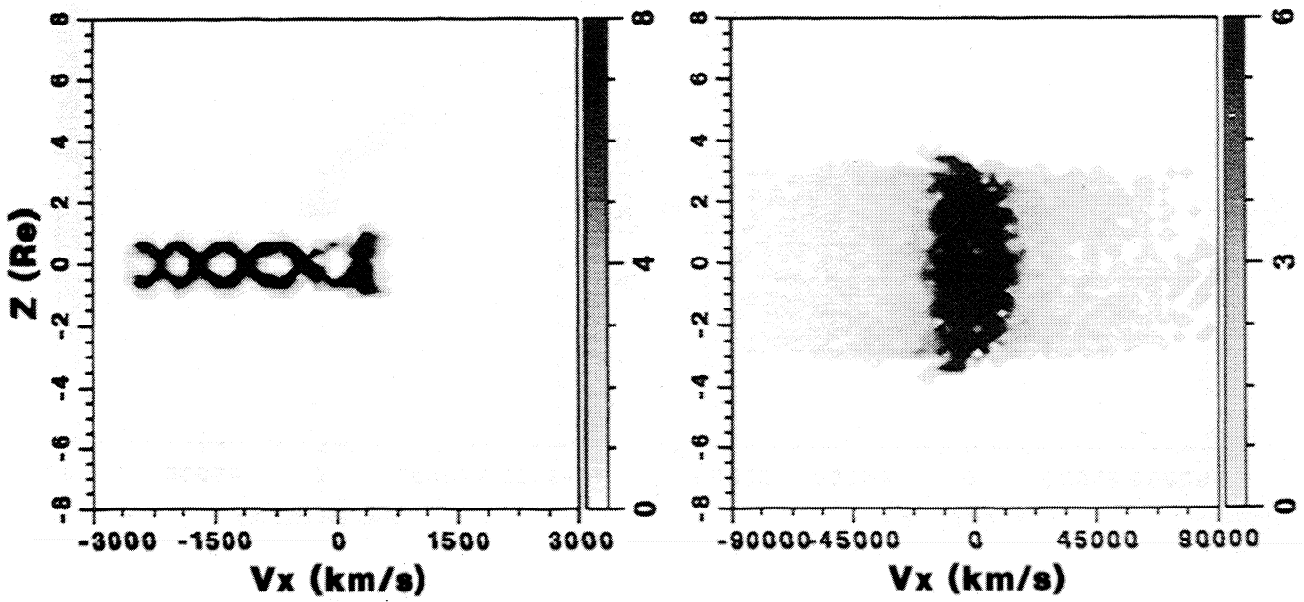

Figure 7. Phase space contours at $x = 70\ R_E$ in the magnetotail for (left) ions and (right) electrons. They are plotted in the z–v_x plane in the same format as Figures 4 and 6.

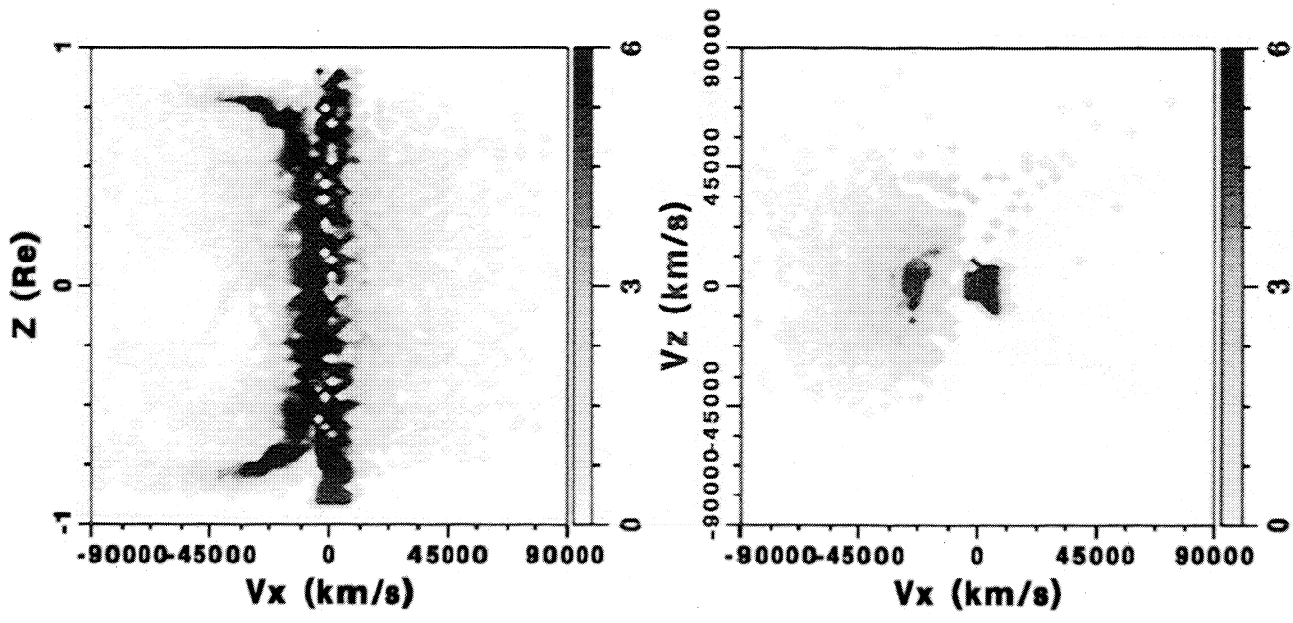

Figure 8. (left) Phase space contours of electrons at $x = 90\ R_E$ and (right) velocity space in the v_z–v_x plane taken at $x = 90\ R_E$, $z = 0.8\ R_E$, which corresponds to the plasma sheet boundary layer. The scale of z on the plot on the left is from +1 to -1 R_E, while the velocity scales are in units of km/s ranging from -90,000 to +90,000 km/s. An earthward streaming beam can be seen in the velocity space plot on the right panel.

how the highly skewed electron distribution is formed can be found in the previously mentioned references (in particular, that of *Dungey* [1988]) and is essentially due to large gyro-orbit motion about the weak normal magnetic component in the x–y plane. The highly nonisotropic, nongyrotropic nature of the skewed electron distribution seen in Figure 9 suggests some plasma instability could result [*Motschmann and Glassmeier*, 1993; *Convery et al.*, 1998; *Motschmann et al.*, 1998], which would most likely modify the distribution by wave-particle interactions and could play a role in anomalous resistivity. A detailed analysis needs to be done to determine the types of waves that could be unstable before any further discussion can proceed.

A major result of the numerical calculations are the ion and electron temperatures in the central plasma sheet and the ratio T_i/T_e. Figure 10 shows a plot of the ion and electron tempera-

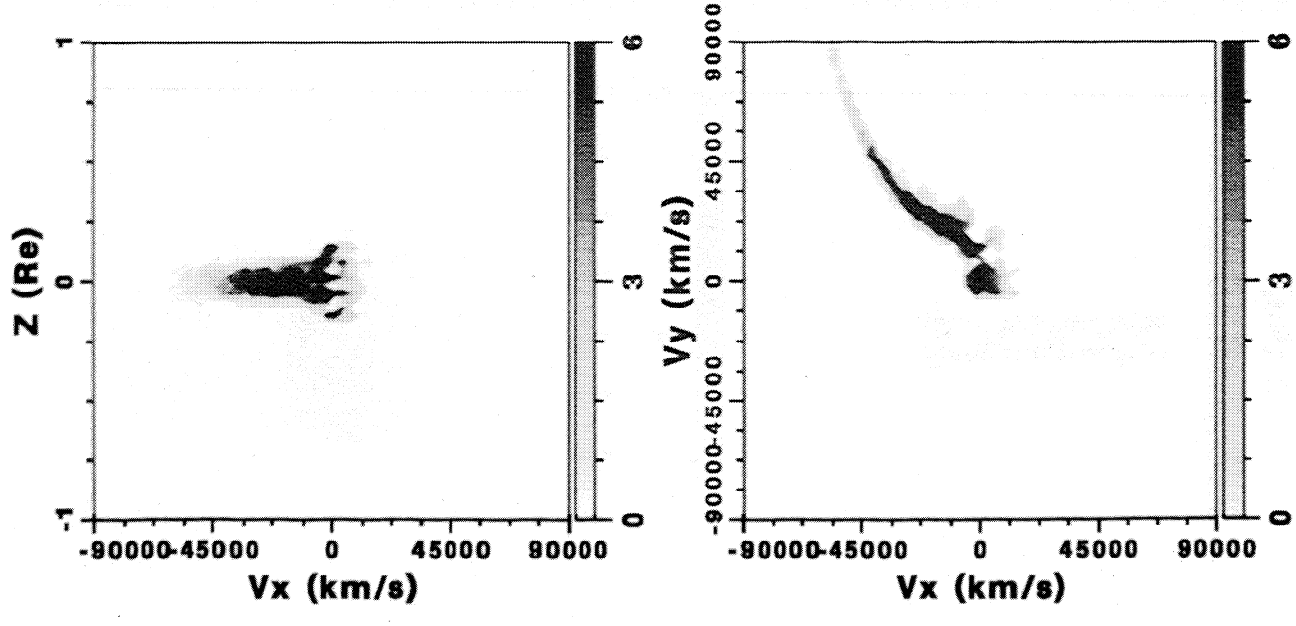

Figure 9. (left) Phase space contour of electrons at $x = 97\ R_E$ and (right) a plot of velocity space in the v_y–v_z plane at $x = 97\ R_E$, $z = 0\ R_E$ in a format similar to Figure 8. The left panel shows electron jetting earthward from the X line, while the right panel shows a highly skewed velocity space distribution in the magnetotail midplane in the transverse direction. Note that at $z = 0$ the magnetic field is in the z direction and thus x and y are transverse to B.

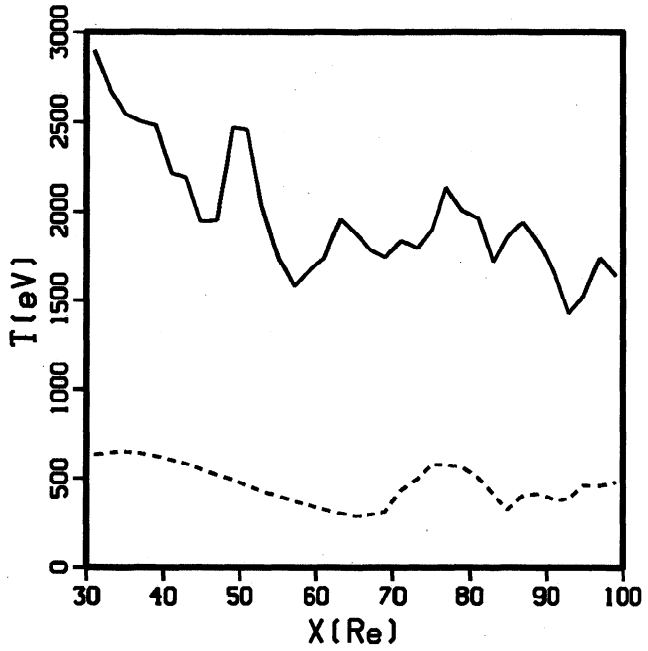

Figure 10. Temperature in eV plotted in the magnetotail midplane versus downtail distance x for protons (solid line) and electrons (dashed line). Temperature is calculated by taking the moment of the distribution from the $z = 0$ virtual detector every 1 R_E in x.

tures versus x down the magnetotail in the CPS at $z = 0$. The ion temperature is shown by the solid line and the electron temperature is shown by the dashed line. The temperatures are shown in eV and are found by taking moments of the distribution function [*Ashour-Abdalla et al.*, 1994]. It must be kept in mind that although temperature is usually considered a measure of a Maxwellian distribution function thermal width, the CPS distributions here are better fit to a power law high-energy tail distribution as already discussed. Figure 10 shows that ion temperatures (solid line) range between about 2 and 3 keV, with higher temperatures nearer to the Earth. Beyond about 70 R_E, ion distributions are highly nonisotropic as indicated in Figure 7, and the meaning of temperature becomes somewhat unclear. The increase in ion temperature earthward of about 45 R_E is due in part to adiabatic radius of curvature and grad B drift in the cross-tail duskward direction. Electron temperatures (dashed curve) range between about 300 and 600 eV. The bump in electron temperature between 70 and 85 R_E downtail occurs in the region of transition between nonadiabatic motion tailward of 85 R_E and adiabatic motion earthward of 70 R_E. The steady increase in electron temperature earthward of 70 R_E is due to adiabatic energization as the electrons convect earthward and experience radius of curvature and grad B drifts, as did the ions earthward of about 45 R_E.

The delineation between adiabatic and nonadiabatic motion for electrons can be determined by calculating the κ parameter for adiabaticity [*Büchner and Zelenyi*, 1989], which is a measure approximately of magnetic field to particle energy. This κ parameter will be discussed in detail in the next section and should not be confused with kappa used by *Christon et al.* [1988] to describe power law distribution functions that we have discussed earlier in this section. It has been shown that approximately where $\kappa > 1$, particle motion is adiabatic and where $\kappa < 1$, motion is approximately nonadiabatic. Tailward of about 85 R_E in the field reversal region, we have found that most electrons have $\kappa < 1$, and thus motion is predominantly nonadiabatic, while earthward of 70 R_E, $\kappa >> 1$ and adiabatic motion dominates. In the region between about 70 and 85 R_E, there is a mixture of these particles and many have $\kappa \sim 1$. Thus the motion is chaotic and difficult to describe analytically. A similar delineation occurs for ions much closer to the Earth at about 10 to 20 R_E. Please see *Ashour-Abdalla et al.* [1992, 1993] for the details and the consequences of this delineation for ions.

The fluctuations in the ion and electron temperature versus downtail distance seen in Figure 10 are due to losses of particles at the magnetopause boundary. If ions or electrons cross the magnetotail midplane for the first time at particular locations, they can follow nonadiabatic Speiser trajectories (see next section for details concerning these trajectories) and are strongly accelerated by the cross-tail electric field in y. A significant number of these Speiser particles hit the magnetopause boundary which we have placed at $|y| = 25$ R_E and are considered lost from the system. This extraction of energetic particles lost at the y boundary for particular x locations can result in the temperature (energy) fluctuations seen in Figure 10. This effect was originally seen for ions in the study by *Ashour-Abdalla et al.* [1994] and is reproduced here. The results in Figure 10 show that electrons also exhibit this effect deeper in the magnetotail where electron nonadiabatic motion occurs (tailward of 70 R_E). Observed electron temperature profiles in the plasma sheet versus downtail distance tailward of about 40 R_E by *Slavin et al.* [1985] also show "bumps" in electron temperature somewhat similar to that seen in Figure 10, although we cannot state for certain that the two features are related. Unfortunately, there was no ion data taken by the ISEE 3 satellite so we cannot compare with a similar profile for the ion temperature. Perhaps Geotail data (which includes both ions and electrons) can be used for comparison at some time in the future when statistical results of this kind are available.

The ion to electron temperature ratio (T_i/T_e) in the CPS versus distance down the magnetotail is shown in Figure 11. The value ranges between about 4 and 6, which is comparable to the middle range of observed values. For example, *Frank* [1985] quoted a value of T_i/T_e between 3 and 5, while *Slavin et al.* [1985] gave a value of $T_i/T_e = 7.8$ from 30 to 60 R_E, 6.7 from 60 to 100 R_E, and less than 4.8 tailward of 100 R_E downtail. Nearer to the Earth, *Baumjohann et al.* [1989] found a best fit of $T_i/T_e = 7.8$ to the AMPTE data. More recent Geotail satellite observations give values of T_i/T_e of about 5 tailward of 30 R_E [*Paterson and Frank*, 1994]. Since these observations were made at different times and with different satellites, it is not surprising that there is variability in the measured values of T_i/T_e, but it can safely be concluded that the average ion temperature is larger than the electron temperature in the magnetotail plasma sheet, usually by a factor of at least 3 to 4. The numerical trajectory calculations, as seen in Figure 11, are consistent with these observations indicating that single particle motion in a magnetotail type field reversal geometry results naturally in $T_i > T_e$ throughout the heated CPS. This claim is discussed further using basic analytic single-particle trajectory arguments in the next section.

It should be noted that in Figures 10 and 11 the temperatures are averaged over the perpendicular and parallel directions. In some locations of the central plasma sheet where particle motion is predominantly adiabatic, the numerical results show

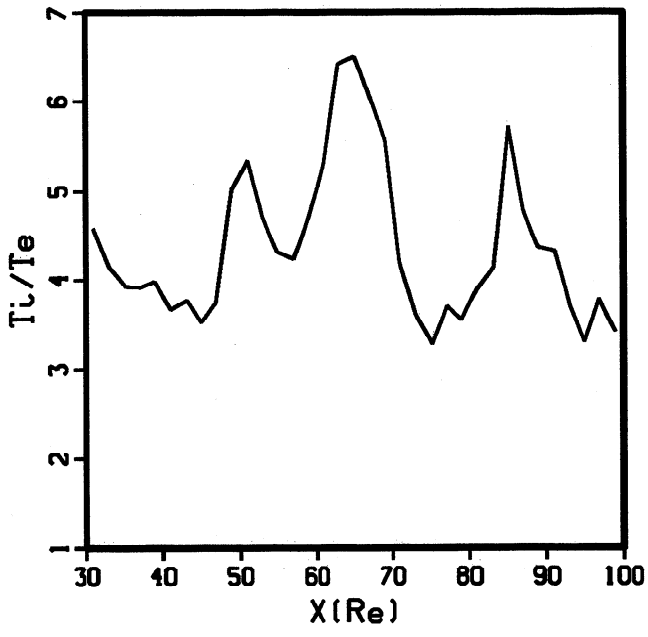

Figure 11. The ion to electron temperature ratio T_i/T_e at $z = 0$ versus distance down the magnetotail in x away from the Earth.

temperature anisotropies such that $T_\perp > T_\parallel$ by a factor of about 1.5 to 2. Since we wanted to compare our results with statistical observations of temperatures from different satellites, which are almost always given in terms of T (rather than by components), we used the average temperature. The increase in perpendicular energy is a consequence of adiabatic motion and earthward plasma convection in the presence of the cross-tail electric field and has been seen in previous numerical results for ions in the near-Earth region at $x < 10\ R_E$ [*Ashour-Abdalla et al.*, 1994].

5. Analytic Expression for T_i/T_e in a Magnetotail-like Geometry

In this section we discuss current sheet acceleration [*Cowley*, 1984] and nonadiabatic particle motion [*Büchner and Zelenyi*, 1989] as a means of forming the quiet time heated central plasma sheet (CPS). Using these ideas for both ions and electrons in a magnetotail field reversal geometry, an analytic expression for the ion to electron temperature ratio is derived. It should be noted that the expression to be derived applies to any magnetic field model with a current sheet field reversal configuration and a monotonically decreasing normal magnetic field component.

When a charged particle crosses the midplane of the plasma sheet where the magnetic field reverses direction, energization can occur due to the cross-tail convection electric field [*Speiser*, 1965a, b; *Dungey*, 1968]. This can result in an energy gain of up to several keV for relatively cool (< keV) inflowing ions. Electrons are not accelerated to the same extent as ions in a current sheet geometry [*Speiser*, 1965a; *Cowley*, 1984] and thus would not be expected to be as energetic as ions in the plasma sheet. This basic concept is used here to explain the difference in ion and electron temperatures in the plasma sheet.

The breakdown of adiabatic invariance in the field reversal region of the magnetotail can contribute to the formation of an energized plasma sheet [*Sonnerup*, 1971; *Birmingham*, 1984; *Chen and Palmadesso*, 1986; *Büchner and Zelenyi*, 1986]. When this happens, various types of particle orbits are possible, and weak or strong chaotic motion can ensue [*Büchner and Zelenyi*, 1989; Chen, 1992]. Some of the energized particles follow a "Speiser" trajectory and go on to form beams in the plasma sheet boundary layer (PSBL) [*Lyons and Speiser*, 1982], while others with so-called "trapped" trajectories remain in the CPS region and form a heated plasma population [*Ashour-Abdalla et al.*, 1991b, 1993].

In a review of plasma acceleration in the Earth's geomagnetic tail, *Cowley* [1984] showed analytically that the speed v_1 a charged particle attains after passing through a simple one-dimensional magnetotail current sheet with a field reversal geometry in the midplane is:

$$v_1 \approx \frac{2E_y}{B_n} + v_0 \tag{2a}$$

where E_y is the cross-tail convection electric field, B_n is the normal field component in the midplane of the current sheet, and v_0 is the initial velocity of a particle entering the current sheet. The magnetic field is assumed to be symmetric around $z = 0$ with $B_y = 0$. In the equatorial magnetic midplane, $B_x = 0$ and the normal magnetic field component is $B_n = B_z$. For this model, at the magnetotail midplane the magnetic field B_n along any field line is at a minimum and the convection velocity (E_y/B_n) maximizes. At locations deep in the magnetotail where B_n is relatively small, current sheet acceleration as represented by (2a) can be quite significant.

The result in (2a) is true only if the incoming particle's velocity is essentially field aligned, it suffers very little change in pitch angle when crossing the current sheet, and exits the current sheet field aligned. If pitch angle scattering occurs when the particle crosses the current sheet (say due to some nonadiabatic process), the particle will still gain energy during the current sheet crossing, but not as much [*Cowley*, 1978, 1984]. In the limit the particle goes from zero degree pitch angle to 90° pitch angle during the current sheet crossing, the speed the particle will have after exiting the current sheet will be:

$$v_1 \approx \frac{\sqrt{2}E_y}{B_n} + v_0 \tag{2b}$$

which is similar to the result in (2a) except that the numerical factor 2 is replaced by $\sqrt{2}$. This follows directly from (19) of *Cowley* [1978] taking the outgoing pitch angle to be 90° and equating the displacement in y that the particle undergoes during the current sheet interaction with the energy gain the particle receives (i.e., $W = qE_y\,\Delta y$).

When plasma first enters the closed field line region of the magnetotail from the lobe or mantle, it is relatively cool with temperatures of at most a few hundred eV. The motion of this cool source plasma is predominantly field aligned combined with $E \times B$ convection towards the midplane of the magnetotail [*Pilipp and Morfill*, 1978]. The energy of an incoming charged particle just before it crosses the midplane of the current sheet can be written as

$$W_0 = \frac{1}{2}m\left[\left(E_y/B_n\right) + v_0\right]^2 \tag{3}$$

where m is the particle mass. In (2a), (2b), and (3), the convection term will be dominant, that is, $E_y/B_n > v_0$, in the magnetotail midplane for initially cool inflowing plasma where B_n is relatively small (in the deep tail region beyond about 30 R_E). While for ions this occurs over most of the magnetotail tailward of 30 R_E, electrons must cross the magnetotail midplane fairly close to the X line region where the magnetic field is very weak in order for the E_y/B_n term to be relatively large. For example, at $x = 95$ R_E the $B_n \approx 0.05$ nT (from the *Tsyganenko* [1989] field model) and for $|E_y| = 0.25$ mV/m, $E_y/B_n = 5000$ km/s. Thus lobe electrons with incoming energies less than 50 eV (speed $\approx$ 4000 km/s) will have $E_y/B_n > v_0$. For electrons the regions in the magnetotail midplane where this occurs is spatially limited (compared to ions), but this is the particular region that we consider here which coincides with the region of nonadiabatic motion for electrons.

The sources we have considered in this paper are either the mantle or lobe, and many particles from these source regions satisfy the conditions necessary to make (2a), (2b), or (3) valid. As previously stated in section 2, we did not consider a low-latitude boundary layer (LLBL) source in this paper since our field model is two-dimensional in the x–z plane. Particles from the LLBL may not satisfy the conditions discussed here, that is, initially relatively cool with motion dominated by $E \times B$ convection and field-aligned streaming, and thus the following formalism cannot necessarily be applied for LLBL particles. How much of the plasma sheet is populated by the different sources (mantle, lobe, LLBL) is not entirely clear and future studies both numerical and analytical should take this into consideration.

The motion of a particle in the magnetotail field reversal region can be categorized using the κ parameter, defined as [*Büchner and Zelenyi*, 1989]

$$\kappa = \sqrt{\frac{R(x)}{\rho_n}} \tag{4a}$$

where $R(x)$ is the radius of curvature of the magnetic field at the x position where the particle crosses the field reversal plane and ρ_n is the particle gyroradius taken at this same point. The κ in (4a) and used in the rest of this section should not be confused with the kappa parameter used by *Christon et al.* [1988] to characterize particle distribution functions with a high-energy tail. If $\kappa >> 1$, the particle behavior is generally adiabatic, whereas when $\kappa \lesssim 1$, the particle will tend to behave nonadiabatically or quasi-adiabatically [*Büchner and Zelenyi*, 1989]. Details on the motion exhibited by particles with $\kappa \sim 1$ and parameter dependences of this motion are given by *Delcourt et al.* [1996a]. For simplicity we assume that for $\kappa \lesssim 1$, the particle behaves non-adiabatically. A more rigorous derivation should take into account the parameter dependencies discussed by *Delcourt et al.* [1996a].

The gyroradius of a charged particle the first time it crosses the field reversal plane is given by

$$\rho_n = \frac{1}{\Omega_n}\sqrt{\frac{2W_0}{m}} = \frac{\sqrt{2mW_0}}{qB_n}$$

where $\Omega_n = q\,B_n/m$ is the cyclotron frequency. Using this expression for ρ_n, κ can be written as

$$\kappa = \left(\frac{1}{2mW_0}\right)^{1/4}\sqrt{qB_nR(x)} \tag{4b}$$

Since we are concerned here with temperatures in the central plasma sheet, we are interested in the particles that form the heated CPS. These particles exit the current sheet region with a relatively large pitch angle and follow trapped orbits. This is in contrast to the Speiser particles, which after being accelerated in the current sheet have small pitch angles and move along high-latitude field lines and form beam distributions in the PSBL. An example of both a trapped proton and a Speiser proton are presented in Figure 12, which shows on the top panels the trajectory of each type of particle projected into the noon-midnight meridian (z versus x). Below each of the trajectories is an energy versus time profile of the particle. In Figure 12 it can be seen that after both particles are launched from $x = 15$ R_E, $z = 8$ R_E, they move tailward and convect towards the equatorial plane. The particles cross $z = 0$ (magnetotail midplane) at different x locations and after their first current sheet interaction follow very different types of trajectories. The left two panels show the Speiser particle, which is energized in the current sheet from an initial energy of ~ 1 keV up to ~ 22 keV, then exits the equatorial region and streams towards the Earth along a high-latitude field line; this is a "classic" Speiser trajectory and these types of protons can form field-aligned beams in the PSBL [*Lyons and Speiser*, 1982]. The particle shown in the right panels of Figure 12 follows a different type of trajectory, and after its first current sheet interaction it stays in the plasma sheet region near $z = 0$ as it convects earthward; the final energy of this trapped particle seen in the lower right panel is about 5 keV which represents a factor of 10 increase over its initial energy of ~ 500 eV. The energy of the trapped proton after being accelerated in the current sheet is typical of ions in the CPS.

Electrons exhibit similar trajectories as those seen for ions and are shown in Figure 13 [see *Schriver and Ashour-Abdalla*, 1994, Figure 4]. To undergo this type of acceleration, electrons must cross the magnetic midplane further down the magnetotail compared to protons where the normal magnetic field is weaker. Comparing Figure 13 with Figure 12, which plot the same quantities in each of the four panels but on different scales, notice that for the electrons the first crossing of the magnetotail midplane at $z = 0$ and the resultant energization occurs at about 97 R_E, whereas the proton acceleration shown in Figure 12 occurs earthward of 80 R_E. Apart from where the energization occurs, however, qualitatively the types of orbits, either Speiser or trapped are similar for ions and electrons and the basic physical explanation for the two types of orbits is the same.

Whether an ion or electron follows a trapped orbit or a Speiser orbit as shown in Figures 12 and 13 depends on the particle's κ upon the first $z = 0$ crossing. The trapped particles have a κ that satisfies:

$$\kappa_t \approx \frac{C}{N} \tag{5a}$$

where $C \approx 0.8$ [*Büchner*, 1991; *Ashour-Abdalla et al.*, 1993] and N is an integer (N = 1,2,3...). Particles that follow Speiser trajectories have a different κ value that instead satisfies

$$\kappa_s \approx \frac{C}{N+1/2} \tag{5b}$$

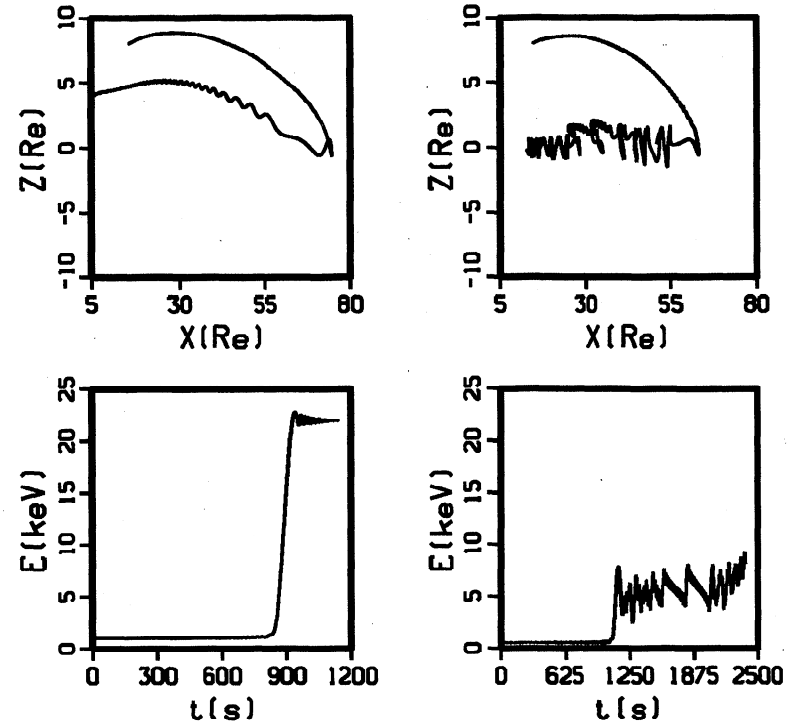

Figure 12. This plot shows the trajectory projected in the noon-midnight meridian (z–x plane) of two different protons launched tailward from the mantle region in the *Tsyganenko* [1989] magnetic field model. (left top) Path of a Speiser particle and (right top) path of a trapped particle orbit. The energy-time history of each particle is shown below the trajectory. Both particles are energized during their first crossings of the magnetotail midplane ($z = 0$), but the details of each trajectory are very different and depend on the particle's κ at the initial $z = 0$ crossing location.

as discussed by *Büchner* [1991], *Chen* [1992], and *Ashour-Abdalla et al.* [1993]. The factor C in (5a) and (5b) is taken here as a constant, but C does have a weak and complex pitch angle dependence [*Büchner*, 1991; *Ashour-Abdalla et al.*, 1993]. For tractability we will assume here that C is a constant given by 0.8. The different classes of orbits have been shown to occupy different regions of phase space and can form distinct features in the resulting velocity distribution functions [*Chen and Palmadesso*, 1986; *Burkhart and Chen*, 1991].

The criteria given by (5a) selects the particles that form the heated CPS. We now estimate the temperature of the plasma made up of these particles. Setting the right-hand side of (5a) equal to the right-hand side of (4b) gives

$$\kappa_t = \frac{C}{N} = \left(\frac{1}{2mW_0}\right)^{1/4} \sqrt{qB_n R(x)} \tag{5c}$$

Now we can use (3) to eliminate W_0 and (2b) to eliminate B_n. We use (2b) since we are interested in trapped particles which can experience a large amount of pitch angle scattering while being energized in the current sheet. Neglecting the relatively small v_0 terms in (2b) and (3), and making these substitutions gives

$$\frac{C}{N} = \sqrt{\frac{2qE_y R(x)}{mv_1^2}} \tag{5d}$$

Solving for v_1 gives the typical speed for trapped particle after the first current sheet interaction:

$$v_1 = \left(\frac{N}{C}\right)\sqrt{\frac{2qE_y R(x)}{m}} \tag{6}$$

The typical energy of the CPS particles for a particular N value will then be given by

$$W_{\mathrm{CPS}} = \frac{1}{2}mv_1^2 = \frac{qE_y N^2 R(x)}{C^2} \approx 1.6\, N^2 qE_y R(x) \tag{7a}$$

using the numerical value $C = 0.8$ according to *Büchner* [1991] and *Ashour-Abdalla et al.* [1993]. The energy given by (7a) depends on the local cross-tail electric field and the radius of curvature at the point where the particle crosses the magnetotail equatorial plane. A similar result can also be found by assuming the energy gain by a particle during a current sheet interaction is given by

$$W = qE_y \Delta y = qE_y 2\rho_n \tag{7b}$$

as discussed by *Cowley* [1984]. This last expression was obtained by assuming that the translational motion Δy, of a particle as it gains energy from the electric field will be $2\rho_n$

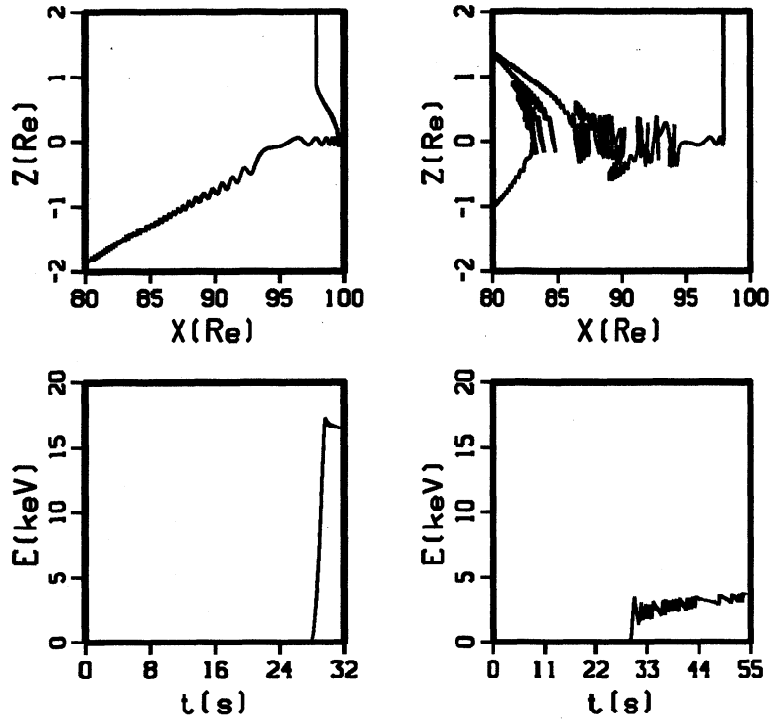

Figure 13. This plot is similar to Figure 12 except here electron trajectories are shown. The four panels here show the same quantities as the four panels in Figure 12, except here the scales are different in the top panels. Here a region much closer to the X line near 100 R_E is shown compared to Figure 12, and the z scale is from –2 to +2 (rather than ± 10 as shown in Figure 12).

[*Chen*, 1992]; eliminating ρ_n by using (4) and (5) then gives (7a).

An explicit mass dependence in (7a) can be revealed by using the radius of curvature for a simple two-dimensional parabolic current sheet model in the x–z plane with $B_y = 0$ [see, e.g., *Büchner and Zelenyi*, 1989]

$$R(x) \approx \frac{B_z}{\partial B_x / \partial s} = \frac{B_n(x)}{B'(x)}$$

where s is the direction along the field line. In the magnetotail midplane, B_z is the normal magnetic field, that is, $B_z = B_n$, and we define $B' = \partial B_x / \partial s$. Note that we assume B_n varies with x along the current sheet and B' also has an x dependence. By using the above expression for $R(x)$ in (7a) and eliminating B_n by use of (2b), we obtain

$$W_{\mathrm{CPS}} = m^{1/3}(1.26E_y N)^{4/3}(q/B')^{2/3} \tag{7c}$$

Finally, assuming the energy of plasma sheet particles in (7c) is an approximate measure of temperature, the ion to electron temperature ratio can be found as

$$\frac{T_i}{T_e} = \left(\frac{m_i}{m_e}\right)^{1/3}\left(\frac{B_e'}{B_i'}\right)^{2/3} \tag{8}$$

where the subscripts on B' represents the field gradient at the location where either ions or electrons first cross the magnetotail midplane and are accelerated nonadiabatically. Equation (8) shows explicitly that T_i/T_e depends on the ion to electron mass ratio to the one-third power (which for protons is $(m_i/m_e)^{1/3}$ = 12.2) and the factor depending on the magnetic field gradient at the locations of electron and ion nonadiabatic acceleration at the first crossing of the magnetotail midplane. Although (8) shows an explicit mass dependence, the magnetic gradient factor contains an implicit mass dependence as well since ions and electrons are accelerated at different locations in the magnetotail.

Equation (8), which gives T_i/T_e, assumes that ions and electrons are accelerated at different locations, and thus strictly speaking is valid earthward of the most earthward acceleration region. For example,if electrons are accelerated nonadiabatically tailward of about 85 R_E, giving rise to the T_e in (8), while ions are accelerated through nonadiabatic means primarily tailward of 40 R_E, giving rise to T_i, then (8) for T_i/T_e would only hold earthward of 40 R_E where both species have been accelerated and convected earthward. This also assumes that any adiabatic energization of electrons that occurs as they convect earthward is negligible compared to the energy gain they initially received as a result of the nonadiabatic acceleration. Tailward of 40 R_E, which is within the region of nonadiabatic ion acceleration, the picture gets muddled and the validity of (8) with the assumptions we have used becomes questionable. It is interesting to note, however, that the numerical results presented in Figure 11 show a relatively consistent value of T_i/T_e down the length of the entire magnetotail between about 30 and 100 R_E, even though (8) is valid only earthward of about 40 to 45 R_E.

To derive (8) for the ion and electron temperatures, we have considered that all of the energy gain of the particles occurs during the first neutral sheet crossing. The justification for this

comes from looking at numerous particle trajectories such as those shown in Figure 12 and 13. Looking at these figures it can be seen for the particles shown in each case that there is a big increase in energy which corresponds to the first crossing of the magnetotail midplane. This is not to say that the particles cannot gain more energy after the first crossing or that every single particle behaves exactly this way, but the majority of particles (ions and electrons) that we have examined that cross the midplane the first time where nonadiabatic motion dominates receive the largest jolt of energy at that location with usually only relatively negligible additional energization after that. One reason for this is because for the plasma sources we use, the particles first enter the plasma sheet location relatively cool moving along the field line from larger $|z|$ values towards $z = 0$ and cross the magnetotail midplane at their furthest tailward x location where B_n is smallest (for that particle) and the energy gain is largest according to (2a) or (2b).

We have assumed that when we take the ratio T_i/T_e, E_y is uniform down the magnetotail. If this is not the case then the E_y terms will not necessarily cancel, and knowledge of the local electric field must be obtained. The general results of this section should still apply as long as E_y varies slowly within the electron and ion acceleration region. In general, our calculations for this paper only hold as long as conditions in the magnetotail are quasi-static for at least about 30 min. This is about how long it takes for the slowest ions to reach the plasma sheet from the source region, get accelerated, and leave the system. Changes in the field configuration on timescales less than this cannot be treated within our theoretical framework.

Another assumption that has gone into deriving (8) is that the primary contribution to the CPS from the nonadiabatic trapped particles is from the same N value for ions and electrons. The CPS will, of course, have ions and electrons from many N values. Analysis of particles in the CPS in our numerical calculations show that the lower N values contribute the most particles because those are broader in x. The same is true for both ions and electrons. A more rigorous calculation would involve summing the contribution of particles from all of the N values.

A numerical value for (8) can be found using B' from the T89 model. Assuming ions are non-adiabatically accelerated at $N = 1$ in the magnetotail, which is at about $x = 40\ R_E$ downtail, and electrons are also accelerated at $N = 1$, which occurs at about $x = 90\ R_E$ downtail, the T89 model gives $B_i'(x = 40\ R_E) = 3.01$ nT/R_E and $B_e'(x = 90\ R_E) = 0.73$ nT/R_E. Using these values in (8) gives $T_i/T_e = 4.8$ which would be valid for locations earthward of 40 R_E. This is a good estimate of the numerical trajectory calculations in the previous section. It is interesting to note that equation (8) for T_i/T_e depends only on the ion to electron mass ratio to the one-third power and a factor depending on the gradients of the field. Thus as long as the normal magnetic field decreases with distance in the magnetotail to small values, (8) will roughly hold. The magnetic field does not have to actually vanish, but in order for electrons to exhibit nonadiabatic motion, defined here loosely to be when $\kappa \approx 1$, the normal magnetic field must have values $\lesssim 0.1$ nT in the magnetotail.

6. Summary and Conclusion

Proton and electron trajectories have been followed from relatively cool (< 300 eV) source regions in the lobe and mantle through the quiet time *Tsyganenko* [1989] magnetotail field model with a constant cross-tail electric field. Calculations of the distribution functions at different locations lead to a qualitative picture of the central plasma sheet that is in approximate agreement with observations. Many previous studies have examined proton motion in the magnetotail, so the focus here is on electrons and comparisons with protons. The main results from the numerical calculations are the following.

1. The heated plasma sheet that forms due to adiabatic and nonadiabatic motion has an ion temperature larger than the electron temperature with the ratio $T_i/T_e \approx 5$.

2. Calculated electron distributions throughout the central plasma sheet are better represented by power law high-energy tail distributions than Maxwellians.

3. The electron plasma sheet boundary layer extends further from the neutral sheet and closer to the magnetic separatrix than the ions.

4. Losses of electrons at the magnetopause boundary at particular x locations can lead to temperature fluctuations in the plasma sheet temperature profile versus magnetotail distance.

5. In the weak field region (close to the X line), electron beams are formed, as well as highly skewed distributions in velocity space.

The first three of these results are all in good agreement with well-established statistical observations of the magnetotail.

For the first point concerning $T_i > T_e$, as already discussed, numerous studies using different satellites at different times have found this to be almost always the case in the plasma sheet [*Frank*, 1985; *Slavin et al.*, 1985; *Richardson et al.*, 1987; *Baumjohann et al.*, 1989; *Paterson and Frank*, 1994]. The results found here are due to nonadiabatic acceleration of protons and electrons at different locations in the magnetotail, and an expression has been derived given by (8) which shows that T_i/T_e is proportional to the ion to electron mass ratio to the one-third power and a factor that depends on local field gradients. As long as the normal magnetic field in the magnetotail midplane decreases away from the Earth to low enough values such that electrons exhibit nonadiabatic motion (i.e., $\kappa \lesssim 1$), (8) should hold for relatively quiet times. For incoming electrons of energies ≤ 100 eV, this corresponds to a normal magnetic field of 0.1 nT or less. Figure 2, which shows magnetic field data from the ISEE 3 satellite [from *Slavin et al.*, 1995], indicates that this is true at least some of the time in the deep magnetotail beyond about 100 R_E. As far as we know there is no theory or numerical calculations which have explained why $T_i > T_e$ in the magnetotail up to now.

The second main result is that electron distributions fit better to a high-energy tail type distribution which is in general agreement with the observations of *Christon et al.* [1988, 1989]. The results found in this paper indicate that these types of distributions form naturally as a result of adiabatic and nonadiabatic motion in a magnetotail-like configuration.

The third result is that the electron plasma sheet boundary layer is found at higher latitude field lines than the proton plasma sheet boundary layer. Thus as a satellite moves from the lobe towards the plasma sheet, just after crossing the separatrix into the closed field line region, energized electrons will be observed first and then deeper into the plasma sheet boundary layer accelerated ions will be observed. This is the picture which emerges from observations [*Eastman et al.*, 1984; *Takahashi and Hones*, 1988]. Since we find that most of the particle acceleration occurs deeper in the magnetotail, this result is due mainly to adiabatic motion and time of flight effects as discussed by *Onsager et al.* [1990, 1991].

The fourth result, which can be seen in Figure 10, is that the loss of electrons at the magnetopause boundary, which we placed at $|y| = 25\ R_E$, can lead to temperature fluctuations at particular x locations in the magnetotail. At these particular locations, electrons are strongly accelerated across the magnetotail in y due to nonadiabatic effects and can gain enough energy such that they exit the system through the magnetopause, leading to the energy fluctuations. The same process occurs for ions [*Ashour-Abdalla et al.*, 1994], although it occurs earthward of the electron location, and leads to similar types of fluctuations in the ion energy profile in the magnetotail. Electron temperature fluctuations were reported by *Slavin et al.* [1985] in the deep magnetotail in about the same location as found in Figure 10, although it is difficult to state for certain whether they are caused by the same effects as discussed here.

The fifth result listed above is that field-aligned electron beams are accelerated earthward from the X line region and that very near the X line highly skewed distribution functions are formed in velocity space. These findings confirm previous theoretical results for electron motion near an X line [*Dungey*, 1988; *Lyons and Pridmore-Brown*, 1990, 1992; *Schriver and Ashour-Abdalla*, 1994, 1995; *Smets et al.*, 1996]. Electron beams have been observed in the near-Earth PSBL [*Parks et al.*, 1984; *Onsager et al.*, 1990, 1991], and measurements of electrostatic solitary waves (ESW) by the Geotail satellite [*Matsumoto et al.*, 1994], which are most likely driven by electron beams [*Omura et al.*, 1994, 1996], provide indirect evidence for the existence of electron beams in the deep magnetotail. There is no existing observational evidence of highly skewed electron velocity distributions in the magnetotail plasma sheet. One possible reason for this is that since these distributions are expected to occur only in the immediate vicinity of an X line it could be rare that a satellite encounters this region. Another possibility is that wave-particle interactions driven by nongyrotropic distributions thermalize the distribution [*Motschmann and Glassmeier*, 1993; *Convery et al.*, 1998; *Motschmann et al.*, 1998]. It is also possible that the influence of ambipolar fields or time variation effects, both of which we have neglected here, prevents the formation of these distributions in the local region near the X line. More detailed theoretical studies which includes these effects need to be carried out before a definitive conclusion can be reached.

Because our results are for quasi-static conditions, we cannot address magnetic substorm acceleration processes, which in general occur on more rapid timescales than the processes discussed here. Induction electric fields play an important role during substorms and a rapidly changing magnetic field configuration can lead to strong ion energization [*Mauk*, 1986; *Delcourt and Moore*, 1992; *Delcourt and Sauvaud*, 1994]. It should also be noted that during quiet times it is possible that particles accelerated during magnetically active periods could still be present and contribute to the plasma sheet. To include these processes, a time-dependent model or simulation would be required. One technique, for example, is to follow charged particle trajectories in a time-changing MHD simulation [*Birn and Hesse*, 1994; *El-Alaoui et al.*, 1998]. To find values for T_i/T_e, however, entire distributions are needed for both ions and electrons.

Another means of heating plasma in the magnetotail which has not been included here are wave-particle interactions. This could be particularly important for cool ions and electrons entering the plasma sheet from the lobe which encounter strong broadband electrostatic noise in the PSBL [*Grabbe and Eastman*, 1984; *Ashour-Abdalla et al.*, 1986; *Schriver and Ashour-Abdalla*, 1987, 1990; *Schriver et al.*, 1990]. Ions can be preferentially heated by low-frequency waves in the PSBL [*Gary and Winske*, 1990] which could contribute to $T_i > T_e$ in the plasma sheet. Whether this occurs is not certain and for the waves suggested by *Gary and Winske* [1990] to be present, a very large density of cold heavy ions would need to be present for the instability to be active. Magnetic noise bursts observed in the magnetotail [*Gurnett et al.*, 1976], which are most likely ion beam generated whistler waves [*Akimoto et al.*, 1987; *Burinskaya et al.*, 1993], could also possibly heat ions in the plasma sheet. It has been shown in general that wave-particle interactions can strongly modify the plasma sheet distribution functions formed by single particle ion trajectory motion under certain conditions [*Holland and Chen*, 1991; *Schriver and Ashour-Abdalla*, 1991]. Thus while it has been shown here that current sheet acceleration by itself can lead to $T_i > T_e$, an important role for wave-particle interactions cannot be ruled out.

It is interesting that the simple model discussed in this paper reproduces basic observed features of the plasma sheet even though self-consistency, wave-particle interactions, and time varying effects are neglected. This suggests that single-particle motion, both adiabatic and nonadiabatic, in the magnetotail field configuration used here naturally leads to a basic plasma sheet as observed. This may indicate that nonadiabatic ion and electron acceleration is a persistent feature of the magnetotail. Despite the promising results found in this study, many observed magnetotail features are not addressed in our model such as substorm injection, bursty bulk flows, plasmoids, and the effect of instabilities. A complete understanding of magnetotail dynamics will have to await simultaneous multipoint satellite observations of the magnetotail along with global self-consistent particle simulations of the region. Until then results from different theoretical approaches and satellite observations must be integrated to form a coherent picture of the nightside magnetosphere.

Acknowledgments. Discussions with L. Zelenyi and V. Peroomian were helpful in the development of this work. This research was supported by the NASA ISTP NAG5-1100 and NSF ATM 94-14760 grants. Computing was performed on the CRAY C90 at the San Diego Supercomputer Center (SDSC). UCLA-IGPP Publication #5076.

The Editor thanks J.-A. Sauvaud and D. Delcourt for their assistance in evaluating this paper.

References

Akimoto, K., S. P. Gary, and N. Omidi, Electron/ion whistler instabilities and magnetic noise bursts, *J. Geophys. Res., 92*, 11209, 1987.

Ashour-Abdalla, M., and H. Okuda, Theory and simulations of broadband electrostatic noise in the geomagnetic tail, *J. Geophys. Res., 91*, 6833, 1986.

Ashour-Abdalla, M., J. Berchem, J. Büchner, and L. M. Zelenyi, Chaotic scattering and acceleration of ions in the Earth's magnetotail, *Geophys. Res. Lett., 17*, 2317, 1990.

Ashour-Abdalla, M., J. Berchem, J. Büchner, and L. M. Zelenyi, Large and small scale structures in the plasma sheet: A signature of chaotic motion and resonance effects, *Geophys. Res. Lett., 18*, 1603, 1991a.

Ashour-Abdalla, M., J. Büchner, and L. M. Zelenyi, The quasi-adiabatic ion distribution in the central plasma sheet and its boundary layer, *J. Geophys. Res., 96*, 1601, 1991b.

Ashour-Abdalla, M., L. M. Zelenyi, J. M. Bosqued, V. Peroomian, Z. Wang, D. Schriver, and R.L. Richard, The formation of the wall region: Consequences in the near Earth magnetotail, *Geophys. Res. Lett., 19*, 1739, 1992.

Ashour-Abdalla, M., J. P. Berchem, J. Büchner, and L. M. Zelenyi, Shaping of the magnetotail from the mantle: Global and local structuring, *J. Geophys. Res., 98*, 5651, 1993.

Ashour-Abdalla, M., L. M. Zelenyi, V. Peroomian, and R. L. Richard, Consequences of magnetotail ion dynamics, *J. Geophys. Res., 99*, 14891, 1994.

Ashour-Abdalla, M., L. A. Frank, W. R. Paterson, V. Peroomian, and L.M. Zelenyi, Proton velocity distribution in the magnetotail: Theory and observations, *J. Geophys. Res., 101*, 2587, 1996a.

Ashour-Abdalla, M., L. M. Zelenyi, V. Peroomian, L. A. Frank, and W. R. Paterson, Coarse-grained texture of ion distributions in the magnetotail: A fractal-like approach, *J. Geophys. Res.*, 101, 15287, 1996b.

Ashour-Abdalla, M., et al., Ion sources and acceleration mechanisms inferred from local distribution functions, *Geophys. Res. Lett., 24*, 955, 1997.

Baker, D. N., S. J. Bame, W.C. Feldman, J. T. Gosling, R. D. Zwickl, J. A. Slavin, and E. J. Smith, Strong electron bidirectional anisotropies in the distant tail: ISEE 3 observations of polar rain, *J. Geophys. Res., 91*, 5637, 1986.

Banks, P. M., and T. E. Holzer, The polar wind, *J. Geophys. Res., 73*, 6846, 1968.

Baumjohann, W., G. Paschmann, and C. A. Cattell, Average plasma properties in the central plasma sheet, *J. Geophys. Res., 94*, 6597, 1989.

Birmingham, T. J., Pitch angle diffusion in the Jovian magnetodisc, *J. Geophys. Res., 89*, 2699, 1984.

Birn, J., and M. Hesse, Particle acceleration in the dynamic magnetotail: Orbits in self-consistent three-dimensional MHD fields, *J. Geophys. Res., 99*, 109, 1994.

Bosqued, J. M., M. Ashour-Abdalla, M. El-Alaoui, V. Peroomian, L. M. Zelenyi, and C. P. Escoubet, Dispersed ion structures at the poleward edge of the auroral oval: Low-altitude observations and numerical modeling, *J. Geophys. Res., 98*, 19181, 1993.

Büchner, J., Correlation-modulated chaotic scattering in the Earth's magnetosphere, *Geophys. Res. Lett., 18*, 1595, 1991.

Büchner, J., and L.M. Zelenyi, Deterministic chaos in the dynamics of charged particles near a magnetic field reversal, *Phys. Lett. A, 118*, 395, 1986.

Büchner, J., and L. M. Zelenyi, Regular and chaotic charged particle motion in magnetotaillike field reversals, 1, Basic theory of trapped motion, *J. Geophys. Res., 94*, 11821, 1989.

Burinskaya, T., D. Schriver, and M. Ashour-Abdalla, The propagation of low-frequency whistler waves driven by ion beams in the magnetotail, *J. Geophys. Res., 98*, 131, 1993.

Burkhart, G. R., and J. Chen, Differential memory in the Earth's magnetotail, *J. Geophys. Res., 96*, 14033, 1991.

Chapman, S. C., Chaotic single particle dynamics in a multi-timescale parameterizable field reversal, *Ann. Geophys., 11*, 239, 1993.

Chapman, S. C., Properties of single-particle dynamics in a parabolic magnetic reversal with general time dependence, *J. Geophys. Res., 99*, 5977, 1994.

Chapman, S. C., and N. W. Watkins, Parameterization of chaotic particle dynamics in a simple time-dependent field reversal, *J. Geophys. Res., 98*, 165, 1993.

Chappell, C. R., T. E. Moore, and J. H. Waite Jr., The ionosphere as a fully adequate source of plasma for the Earth's magnetosphere, *J. Geophys. Res., 92*, 5896, 1987.

Chen, J., Nonlinear dynamics of charged particles in the magnetotail, *J. Geophys. Res., 97*, 15011, 1992.

Chen, J., and P. J. Palmadesso, Chaos and nonlinear dynamics of single-particle orbits in a magnetotaillike magnetic field, *J. Geophys. Res., 91*, 1499, 1986.

Christon, S. P., D. G. Mitchell, D. J. Williams, L. A. Frank, C. Y. Huang, and T. E. Eastman, Energy spectra of plasma sheet ions and electrons from ~ 50 eV/e to ~ 1 MeV during plasma temperature transitions, *J. Geophys. Res., 93*, 2562, 1988.

Christon, S. P., D. J. Williams, D. G. Mitchell, L. A. Frank, and C. Y. Huang, Characteristics of plasma sheet ion and electron populations during undisturbed geomagnetic conditions, *J. Geophys. Res., 94*, 13409, 1989.

Convery, P., M. Ashour-Abdalla, and D. Schriver, Generation of electrostatic waves by nongyrotropic protons, *Adv. Space Res.*, in press, 1998.

Cowley, S. W. H., A note on the motion of charged particles in one-dimensional magnetic current sheets, *Planet. Space Sci., 26*, 539, 1978.

Cowley, S. W. H., The distant geomagnetic tail in theory and observation, in *Magnetic Reconnection in Space and Laboratory Plasmas*, *Geophys. Monogr. Ser.*, vol. 30, edited by E.W. Hones Jr., p. 228, AGU, Washington, D. C., 1984.

DeCoster, R. and L. A. Frank, Observations pertaining to the dynamics of the plasma sheet, *J. Geophys. Res., 84*, 5099, 1979.

Delcourt, D. C., and R. F. Martin Jr., Application of the centrifugal impulse model to particle motion in the near-Earth magnetotail, *J. Geophys. Res., 99*, 23583, 1994.

Delcourt, D. C., and T. E. Moore, Precipitation of ions induced by magnetotail collapse, *J. Geophys. Res., 97*, 6405, 1992.

Delcourt, D. C., and J. A. Sauvaud, Plasma sheet ion energization during dipolarization events, *J. Geophys. Res., 99*, 97, 1994.

Delcourt, D. C., J. A. Sauvaud, and A. Pedersen, Dynamics of single-particle orbits during substorm expansion phase, *J. Geophys. Res., 95*, 20853, 1990.

Delcourt, D. C., J. A. Sauvaud, R. F. Martin Jr., and T. E. Moore, Gyrophase effects in the centrifugal impulse model of particle motion in the magnetotail, *J. Geophys. Res., 100*, 17211, 1995.

Delcourt, D. C., J. A. Sauvaud, R. F. Martin Jr., and T. E. Moore, On the nonadiabatic precipitation of ions from the near-Earth plasma sheet, *J. Geophys. Res., 101*, 17409, 1996a.

Delcourt, D. C., G. Belmont, J. A. Sauvaud, T. E. Moore, and R. F. Martin Jr., Centrifugally driven phase bunching and related current sheet structure in the near-Earth magnetotail, *J. Geophys. Res., 101*, 19,839, 1996b.

Dungey, J. W., Waves and particles in the magnetosphere, in *Physics of the Magnetosphere*, edited by R. L. Carovillano, et al., p. 218, D. Reidel, Hingham, Mass., 1968.

Dungey, J. W., Noise-free neutral sheets, in *Proceedings of the International Workshop on Reconnection in Space Plasma*, vol. II, *Eur. Space Agency Spec. Publ., ESA SP-285*, 15, 1988.

Eastman, T. E., L. A. Frank, W. K. Peterson, and W. Lennartsson, The plasma sheet boundary layer, *J. Geophys. Res.*, 89, 1553, 1984.

Eastman, T. E., B. Popielawska, and L. A. Frank, Three-dimensional plasma observations near the outer magnetospheric boundary, *J. Geophys. Res., 90*, 9519, 1985.

El-Alaoui, M., M. Ashour-Abdalla, J. Raeder, and J. M. Bosqued, Modeling magnetotail ion distributions with global magnetohydrodynamics and ion trajectory calculations, in *Encounter between global observations and models in the ISTP era*, *Geophys. Monogr. Ser.*, AGU, Washington, DC, in press 1998.

Fedder, J. A., J. G. Lyon, S. P. Slinker, and C. M. Mobarry, Topological structure of the magnetotail as a function of interplanetary magnetic field, *J. Geophys. Res., 100*, 3613, 1995.

Frank, L. A., Plasmas in the Earth's magnetotail, *Space Sci. Res., 42*, 211, 1985.

Frank, L. A., K. L. Ackerson, and R. P. Lepping, On hot tenuous plasmas, fireballs, and boundary layers in the Earth's magnetotail, *J. Geophys. Res., 81*, 5859, 1976.

Gary, S. P., and D. Winske, Computer simulations of electromagnetic instabilities in the plasma sheet boundary layer, *J. Geophys. Res., 95*, 8085, 1990.

Grabbe, C. L., and T. E. Eastman, Generation of broadband electrostatic noise by ion beam instabilities in the magnetotail, *J. Geophys. Res., 89*, 3865, 1984.

Gurnett, D. A., L. A. Frank, and R. P. Lepping, Plasma waves in the distant magnetotail, *J. Geophys. Res., 81*, 6059, 1976.

Holland, D. L., and J. Chen, Effects of collisions on the nonlinear particle dynamics in the magnetotail, *Geophys. Res. Lett., 18*, 1579, 1991.

Joyce, G., J. Chen, S. Slinker, D.L. Holland, and J.B. Harold, Particle energization near an X line in the magnetotail based on global MHD fields, *J. Geophys. Res., 100*, 19167, 1995.

Lyons, L. R., Electron energization in the geomagnetic tail current sheet, *J. Geophys. Res., 89*, 5479, 1984.

Lyons, L. R., and D. C. Pridmore-Brown, Force balance near an *X* line in a collisionless plasma, *J. Geophys. Res., 95*, 20903, 1990.

Lyons, L. R., and D. C. Pridmore-Brown, Force balance near an *X* line along which $\mathbf{E} \cdot \mathbf{J} < 0$, *J. Geophys. Res., 97*, 2955, 1992.

Lyons, L. R., and T. W. Speiser, Evidence for current-sheet acceleration in the geomagnetic tail, *J. Geophys. Res., 87*, 2276, 1982.

Martin, R. F., Jr., Chaotic particle dynamics near a two-dimensional magnetic neutral point with applications to the geomagnetic tail, *J. Geophys. Res., 91*, 11,985, 1986.

Martin, R. F., Jr., and T. Speiser, A predicted energetic ion signature of a neutral line in the geomagnetic tail, *J. Geophys. Res., 93*, 11521, 1988.

Matsumoto, H., H. Kojima, T. Miyatake, Y. Omura, M. Okada, and M. Tsutsui, Electrostatic solitary waves (ESW) in the magnetotail: BEN wave forms observed by GEOTAIL, *Geophys. Res. Lett., 21*, 2915, 1994.

Mauk, B. H., Quantitative modeling of the "convective surge" mechanism of ion acceleration, *J. Geophys. Res., 91*, 13423, 1986.

Mead, G. D., and D. H. Fairfield, A quantitative magnetospheric model derived from spacecraft magnetometer data, *J. Geophys. Res., 80*, 523, 1975.

Motschmann, U. M., and K. H. Glassmeier, Nongyrotropic distribution of pickup ion at comet P/Grigg-Skellerup: A possible source of wave activity, *J. Geophys. Res., 98*, 20,977, 1993.

Motschmann, U. M., H. Kafemann, and M. Scholer, Nongyrotropy in magnetoplasmas: Simulation of wave excitation and phase space diffusion, *Ann. Geophys.*, in press, 1998.

Northrup, T. G., *The Adiabatic Motion of Charged Particles*, Wiley-Interscience, New York, 1963.

Omura, Y., H. Kojima, and H. Matsumoto, Computer simulation of electrostatic solitary waves: A nonlinear model of broadband electrostatic noise, *Geophys. Res. Lett., 21*, 2923, 1994.

Omura, Y., H. Matsumoto, T. Miyake, and H. Kojima, Electron beam instabilities as generation mechanism of electrostatic solitary waves in the magnetotail, *J. Geophys. Res., 101*, 2685, 1996.

Onsager, T. G., M. F. Thomsen, J. T. Gosling, and S. J. Bame, Electron distributions in the plasma sheet boundary layer: Time of flight effects, *Geophys. Res. Lett., 17*, 1837, 1990.

Onsager, T. G., M. F. Thomsen, R. C. Elphic, and J. T. Gosling, Model of electron and ion distributions in the plasma sheet boundary layer, *J. Geophys. Res., 96*, 20999, 1991.

Parks, G. K., et al., Particle and field characteristics of the high-latitude plasma sheet boundary layer, J. Geophys. Res., 89, 8885, 1984.

Paterson, W. R., and L. A. Frank, Survey of plasma parameters in Earth's distant magnetotail with the Geotail spacecraft, *Geophys. Res. Lett., 21*, 2971, 1994.

Peredo, M., D. P. Stern, and N. A. Tsyganenko, Are existing magnetospheric models excessively stretched?, *J. Geophys. Res., 98*, 15,343, 1993.

Peroomian, V., and M. Ashour-Abdalla, Population of the near-Earth magnetotail from the auroral zone, *J. Geophys. Res., 101*, 15387, 1996.

Pilipp, W. G., and G. Morfill, The formation of the plasma sheet from plasma mantle dynamics, *J. Geophys. Res., 83*, 5670, 1978.

Press, W. H., B. P. Flannery, S. A. Teukolsky, and W. T. Vetterling, *Numerical Recipes: The Art of Scientific Computing*, Cambridge Univ. Press, New York, 1989.

Raeder, J., R. J. Walker, and M. Ashour-Abdalla, The structure of the distant geomagnetic tail during long periods of northward IMF, *Geophys. Res. Lett., 22*, 349, 1995.

Richard, R. L., R. J. Walker, and M. Ashour-Abdalla, The population of the magnetosphere by solar wind ions when the interplanetary magnetic field is northward, *Geophys. Res. Lett., 21*, 2455, 1994.

Richardson, I. G., S. W. H. Cowley, E. W. Hones Jr., and S.J. Bame, Plasmoid-associated energetic ion bursts in the deep geomagnetic tail: Properties of plasmoids and the postplasmoid plasma sheet, *J. Geophys. Res., 92*, 9997, 1987.

Schriver, D., and M. Ashour-Abdalla, Generation of high-frequency broadband electrostatic noise: The role of cold electrons, *J. Geophys. Res., 92*, 5807, 1987.

Schriver, D., and M. Ashour-Abdalla, Cold plasma heating in the plasma sheet boundary layer: Theory and simulations, *J. Geophys. Res., 95*, 3987, 1990.

Schriver, D., and M. Ashour-Abdalla, Consequences of wave-particle interactions on chaotic acceleration, *Geophys. Res. Lett., 18*, 1607, 1991.

Schriver, D., and M. Ashour-Abdalla, Ion and electron distributions near an *X*-line, in *Proceedings of Second International Conference on Substorm*, p. 503, University of Alaska, Fairbanks, 1994.

Schriver, D., and M. Ashour-Abdalla, Signatures of electron acceleration in the magnetotail, in *Physics of Space Plasmas (1993)*, edited by T. Chang and J.R. Jasperse, p. 403, MIT Cent. for Theor. Geo/Cosmo Plasma Phys., Cambridge, Mass., 1995.

Schriver, D., M. Ashour-Abdalla, R. Treumann, M. Nakamura, and L.M. Kistler, The lobe to plasma sheet boundary layer transition: Theory and observations, *Geophys. Res. Lett., 17*, 2027, 1990.

Slavin, J. A., E. J. Smith, D. G. Sibeck, D. N. Baker, R. D. Zwickl, and S.I. Akasofu, An ISEE 3 study of average and substorm conditions in the distant magnetotail, *J. Geophys. Res., 90*, 10,875, 1985.

Smets, R., D. Delcourt, D. Fontaine, and R. F. Martin Jr., Structure of electron and ion distribution functions near a reconnection line, *J. Geophys. Res., 101*, 24,837, 1996.

Sonnerup, B. U. O., Adiabatic particle orbits in a magnetic null sheet, *J. Geophys. Res., 76*, 8211, 1971.

Speiser, T. W., Particle trajectories in model current sheets, 1, Analytical solutions, *J. Geophys. Res., 70*, 4219, 1965a.

Speiser, T.W., Particle trajectories in a model current based on the open model of the magnetosphere with application to auroral particles, *J. Geophys. Res., 70*, 1,717, 1965b.

Spicer, D. S., S. T. Zalesak, R. Löhner, and S. Curtis, Simulation of the magnetosphere with a new three dimensional MHD code and adaptive mesh refinement: Preliminary results, *Adv. Space Sci., 18(8)*, 253, 1996.

Takahashi, K., and E. W. Hones, Jr., ISEE 1 and 2 observations of ion distributions at the plasma sheet - tail lobe boundary, *J. Geophys. Res., 93*, 8558, 1988.

Tanaka, T., Generation mechanisms for magnetosphere-ionosphere current systems deduced from a three-dimensional MHD simulation of the solar wind-magnetosphere-ionosphere coupling process, *J. Geophys. Res., 100*, 12057, 1995.

Tsyganenko, N. A., Global quantitative models of the geomagnetic field in the cislunar magnetosphere for different disturbance levels, *Planet. Space. Sci., 35*, 1347, 1987.

Tsyganenko, N. A., A magnetospheric magnetic field model with a warped tail current sheet, *Planet. Space Sci., 37*, 5, 1989.

Tsyganenko, N. A., and D. P. Stern, Modeling the global magnetic field of the large-scale Birkeland current system, *J. Geophys. Res., 101*, 27187, 1996.

Tsyganenko, N. A., and A. V. Usmanov, Determination of the magnetospheric current system parameters and development of experimental geomagnetic field models based on data from IMP and HEOS satellites, *Planet. Space Sci., 30*, 985, 1982.

Usadi, A., R. A. Wolf, M. Heinemann, and W. Horton, Does chaos alter the ensemble-averaged drift equations?, *J. Geophys. Res., 101*, 15491, 1996.

Walker, R. J., and T. Ogino, A global magnetohydrodynamic simulation of the origin and evolution of magnetic flux ropes in the magnetotail, *J. Geomagn. and Geoelectr., 48*, 765, 1996.

Walker, R. J., R. L. Richard, T. Ogino, and M. Ashour-Abdalla, Solar wind entry into the magnetosphere when the interplanetary magnetic field is southward, in *Physics of Space Plasmas (1995)*, edited by T. Chang and J. R. Jasperse, p. 561, MIT Cent. for Theor. Geo/Cosmo Plasma Phys., Cambridge, Mass., 1996.

Zelenyi, L. M., A. A. Galeev, and C. F. Kennel, Ion precipitation from the inner plasma sheet due to stochastic diffusion, *J. Geophys. Res., 95*, 3871, 1990.

Zwingman, W., Self-consistent magnetotail theory: Equilibrium structures including arbitrary variation along the tail axis, *J. Geophys. Res., 88*, 9101, 1983.

M. Ashour-Abdalla, R. L. Richard, and D. Schriver, Institute of Geophysics and Planetary Physics, UCLA, 405 Hilgard Avenue, Los Angeles, CA 90095-1567. (e-mail: dave@igpp.ucla.edu)

(Received August 5, 1997; revised December 1, 1997; accepted December 29, 1997.)